Contrib Mineral Petrol (2002) 143: 706–732
DOI 10.1007/s00410-002-0373-6

Teddy Parra · Olivier Vidal · Phillipe Agard

A thermodynamic model for Fe–Mg dioctahedral K white micas using data from phase-equilibrium experiments and natural pelitic assemblages

Received: 1 February 2002 / Accepted: 20 April 2002 / Published online: 9 July 2002

Abstract The purpose of this study is to derive a solid-solution model for potassic white micas (KWM) encountered in rocks of various bulk compositions, over a wide range of P–T conditions. A compilation of phengite compositions lead us to propose a seven-thermodynamic-component (muscovite, Fe^{2+}-Al-celadonite, Mg-Al-celadonite, annite, phlogopite, pyrophyllite and paragonite) ionic solid-solution model which accounts for the Tschermak, Fe–Mg, di/trioctahedral, pyrophyllitic and paragonitic substitutions observed in nature. A four-site mixing model with symmetric Margules parameters to model the Tschermak substitutions, asymmetric Margules parameters to model the other substitutions, and ideal intersite interaction has been adopted. In contrast to previous models, the relevant thermodynamic data and solid-solution properties are calibrated with independent sets of published experiments conducted for the KMASH, KFASH, KFMASH, and KNASH systems, as well as about 200 natural data involving KWM assemblages. The constraints span a wide range of pressure and temperature conditions (150 to 750 °C, 0.5 to 30 kbar), so that our model does not need to be extrapolated outside the calibration range to be used for P–T thermobarometric purposes. The calculated thermodynamic data are interconsistent with the TWQ thermodynamic database and solid-solution models, including that recently published for chlorites.

T. Parra (✉)
Laboratoire de Géologie,
Ecole Normale Supérieure (UMR 8532),
24 Rue Lhomond, 75231 Paris cedex 05, France
E-mail: parra@euclase.ens.fr

O. Vidal
LGCA (UMR 5025),
1381 Rue de la Piscine, BP 53,
38041 Grenoble cedex 09, France

P. Agard
UPMC, Laboratoire de Tectonique,
ESA 70-72, Tour 26, 1 E, Case 129,
4 Place Jussieu, 75252 Paris, France

Editorial responsibility: K. Hodges

Introduction

Dioctahedral potassic white micas (KWM: Rieder et al. 1998) display chemical composition variations which were shown experimentally to depend on thermobarometric conditions (Velde 1965; Chatterjee and Froese 1975; Krogh and Raheim 1978; Green and Hellman 1982; Massonne and Schreyer 1986, 1987; Cathelineau 1988; Cathelineau and Izquerdo 1988; Hynes and Forest 1988; Massonne and Schreyer 1989; Blencoe et al. 1994; Guidotti et al. 1994a, 1994b; Massonne and Szpurka 1997; Guidotti and Sassi 1998b; Schmidt 1998). In the last decade, a considerable amount of natural data bearing on the composition of KWM as a function of pressure (P), temperature (T) and bulk-rock composition also accumulated (see Guidotti and Sassi 1998b for a review). The temperature- or pressure-controlled compositional changes of muscovite and associated phases have led to the formulation of various empirical geothermometers or barometers (see Essene and Peacor 1995 for a review). The most important limitation of the empirical thermometers or barometers is that they are based on only one exchange reaction (e.g., Na–K or Fe^{2+}–Mg) whereas the compositional variability of KWM results from at least six major substitutions (see below). For this reason, the range of compositions for which the empirical thermometers can be used is both limited and questionable (Essene and Peacor 1995; Guidotti and Sassi 1998b). The only way to improve this situation is through the use of thermodynamics. Two models were recently proposed by Massonne and Szpurka (1997) and Holland and Powell (1998), which are compatible with the internally consistent thermodynamic databases of Berman (1988) and Holland and Powell (1998), respectively. In both cases, the composition of KWM is expressed as a linear combination of

Mg-Al-celadonite and muscovite (Holland and Powell 1998), + Fe-Al-celadonite + trioctahedral mica + paragonite + Ti-WM (Massonne 1995; Massonne and Szpurka 1997; cf. Table 1 for abbreviations). Although these models provide new insights on the petrologic significance of KWM, their application for thermobarometric purposes is still limited for the following reasons.

1. The model proposed by Holland and Powell (1998) is a four-site ideal model which does not account for non-ideal K–Na interactions. Therefore, the influence of composition and P–T conditions on the shape of the muscovite–paragonite–pyrophyllite solvi cannot be quantified and compared with natural data. This can be done with Massonne and Szpurka's (1997) non-ideal molecular mixing model. However, Biino and de Capitani (1995) have shown the ambiguity of the ternary term expression for G_{excess} given by Massonne (1995) and later utilized by Massonne and Szpurka (1997). Moreover, the model proposed by Massonne and Szpurka (1997) is constrained only by experiments conducted in the simplified chemical systems KMASH or KFASH. The authors did not consider independent experiments conducted in KFMASH, such as the Fe–Mg partitioning between garnet and phengite (Krogh and Raheim 1978; Green and Hellman 1982), to check the validity of the thermodynamic properties for intermediate Fe–Mg KWM compositions. Also, they did not take into account the substitution(s) responsible for the vacancies in the interfolial site, as discussed below.

Table 1. Abbreviations and structural formula of minerals used in this study. * After Kretz (1983), ** after Holland and Powell (1998)

Mineral	Structural formula	Abbreviation
K white mica solid solution	$(K, Na)_{0-1}(Al, Mg, Fe^{2+})_{2-3}(Si, Al)_4O_{10}(OH)_2$	KWM
Muscovite	$KAl_2(Si_3Al)O_{10}(OH)_2$	Ms*
Mg-Al-celadonite	$K(MgAl)(Si_4)O_{10}(OH)_2$	Mg-ACel
Fe^{2+}-Al-celadonite	$K(Fe^{2+}Al)(Si_4)O_{10}(OH)_2$	Fe^{2+}-ACel
Phlogopite	$KMg_3(Si_3Al)O_{10}(OH)_2$	Phl*
Pyrophyllite	$Al_2(Si_4)O_{10}(OH)_2$	Prl*
Paragonite	$NaAl_2(Si_3Al)O_{10}(OH)_2$	Pg*
Chlorite solid solution	$(Al, Mg, Fe^{2+})_{4-3}(Al, Mg, Fe^{2+})_2(SiAl)_4O_{10}(OH)_8$	Chl
Amesite	$Mg_4Al_2(Si_2Al_2)O_{10}(OH)_8$	Ames**
Clinochlore	$Mg_4(AlMg)(Si_3Al)O_{10}(OH)_8$	Clin**
Daphnite	$Fe^{2+}{}_4(AlFe^{2+})(Si_3Al)O_{10}(OH)_8$	Daph**
Sudoite	$Mg_2Al_3(Si_3Al)O_{10}(OH)_8$	Sud
Garnet solid solution		Gt
Almandine	$Fe^{2+}{}_3Si_3Al_2O_{12}$	Alm*
Pyrope	$Mg_3Si_3Al_2O_{12}$	Pyp*
Grossular	$Ca_3Si_3Al_2O_{12}$	Grs*
Spessartine	$Mn^{2+}{}_3Si_3Al_2O_{12}$	Sps*
Biotite solid solution		Bt
Annite	$KFe^{2+}{}_3(Si_3Al)O_{10}(OH)_2$	Ann*
Phlogopite	$KMg_3(Si_3Al)O_{10}(OH)_2$	Phl*
Chloritoid solid solution		Cld
Fe^{2+}-chloritoid	$Fe^{2+}Al_2SiO_5(OH)_2$	Fe^{2+}-Cld*
Mg-chloritoid	$MgAl_2SiO_5(OH)_2$	Mg-Cld*
Feldspar solid solution		Fd
Potassic feldspar	$K(Si_3Al)O_8$	K-Fd
Albite	$Na(Si_3Al)O_8$	Ab*
Anorthite	$Ca(Si_3Al]O_8$	An*
Others		
Ca-amphiloles	$Ca_2Na_{0-1}(Mg, Fe^{2+}, Fe^{3+}, Al)_5(Si_{6-8}Al_{2-0})O_{22}(OH)_2$	Ca-Amph
Glaucophane	$Na_2Mg_3(Si_8Al_2)O_{22}(OH)_2$	Gln**
Ca-Na-clinopyroxenes	$(Ca, Na)(Mg, Fe^{2+}, Mn, Al)(Si, Al)_2O_6$	Ca-Na-CPx*
Sillimanite	Al_2O_3	Sill*
Andalusite	Al_2O_3	And*
Kyanite	Al_2O_3	Ky*
Mg-carpholite	$MgAl_2Si_2O_6(OH)_4$	Mcar**
Talc	$Mg_3(Si_4)O_{10}(OH)_2$	Tlc*
Quartz	SiO_2	Qtz*
Coesite	SiO_2	Coe*
Water	H_2O	W*

2. The amount of excess Si compared to the ideal number of 3 a.p.f.u. muscovite is assumed to result solely from the Tschermak substitution (TK) between muscovite and Al-celadonite (TK: $Si^{IV} + (Mg + Fe)^{VI} = Al^{IV} + Al^{VI}$). As discussed below, this assumption is probably justified for KWM crystallizing at high T and low P. However, under low-T and high-P conditions, a linear combination of Ms, Fe-ACel, Mg-ACel, Tri and Pg often fails to reproduce the KWM compositions observed in natural samples which show a significant proportion of vacancies, with large Si but low (Fe + Mg) contents (Lambert 1959; Wang and Banno 1987; Frey et al. 1988; Baldelli et al. 1989; Bousquet 1998; Leoni et al. 1998; Agard 1999; Vidal and Parra 2000; Agard et al. 2001). A likely explanation for this combined increase of vacancies and Si content is the existence of the pyrophyllite substitution from muscovite toward pyrophyllite (P: $K^{XII} + Al^{IV} = \square^{XII} + Si^{IV}$; see Guidotti and Sassi 1998a, 1998b for reviews). Hence, for these low-grade KWM, the molar fraction of Al-celadonite and the inferred pressure conditions will be overestimated if calculated from the observed Si content alone (Agard et al. 2001).
3. Phengite is often intimately associated with chlorite in rock microstructures (e.g., Worley et al. 1997; Vidal and Parra 2000; Trotet et al. 2001a, 2001b). Chlorite minerals also show P-T-dependent compositional variations (Vidal et al. 2001), so that P–T conditions can be calculated using chlorite–phengite assemblages (Vidal and Parra 2000). For example, pressure conditions can be estimated from the location of the "Tschermak exchange" reaction between chlorite and phengite at fixed T (i.e., Mg-amesite + Mg-Al-celadonite = muscovite + clinochlore). Such estimates are particularly interesting for rocks devoid of low-variance parageneses. However, available thermodynamic data and solid-solution models for phengite (Massonne and Szpurka 1997; Holland and Powell 1998) were not constrained with equilibria involving chlorite and have not been extensively tested against natural assemblages involving this mineral. For this reason, the compatibility of the chlorite and phengite solid-solution models is questionable.

In this study, we therefore propose a new solid-solution model for KWM and standard-state thermodynamic data for Mg-Al-celadonite and Fe^{2+}-Al-celadonite. In order to minimize the problems mentioned above, the unknown thermodynamic properties are derived from the consideration of (1) experimental results available in the literature for KMASH, KFASH, KFMASH and KNASH systems, and (2) natural data covering a large range of independently known P–T conditions. To ensure compatibility between the chlorite and phengite solid-solution models, a large part of these natural data involves both minerals, and the equilibrium P–T conditions were recalculated using the chlorite model of Vidal et al. (2001).

Provisional thermodynamic data on the KWM solid solution were published by Vidal and Parra (2000). The present model takes into account additional natural and experimental data which help better constrain the solid-solution properties and thermodynamic data of KWM.

Compositional variability and relevant substitutions

The compositional variability of KWM was recently reviewed by Guidotti and Sassi (1998a, 1998b). The most common isomorphous substitutions are listed below (Figs. 1, 2).

1. TK: the Tschermak substitution ($Si^{IV}(Mg, Fe^{2+})^{VI} = Al^{IV}Al^{VI}$), which extends from ideal muscovite to the theoretical Al-celadonite end member, $K(Mg, Fe^{2+})Al(Si_4O_{10})(OH)_2$.
2. Pa: the paragonitic substitution ($K^{XII} = Na^{XII}$), which is limited to KWM-rich and paragonite-poor compositions.
3. FM: the $FeMg_{-1}$ substitution, which is almost complete over the whole range of compositions between Mg- and Fe-Al-celadonite end members.
4. Fe3: the ferrimuscovite substitution ($Al^{VI, VI} = Fe^{3+}$), which can be significant depending on the oxygen fugacity (Guidotti and Yates 1994).
5. P: the deficiency at the XII site, which produces interlayer-deficient, illitic KWM (Rieder et al. 1998). According to Guidotti and Sassi (1998a, 1998b), the alkali deficiency at the XII site can be due to the substitution of K^+ by H_3O^+, NH_4^+ or H_2O, or to the pyrophyllitic substitution (P: $(Na, K)^{XII}Al^{IV} = \square^{XII}Si^{IV}$) from the muscovite–Al-celadonite towards pyrophyllite. For the reasons outlined by Guidotti and Sassi (1998a, 1998b), alkali loss during EMPA analyses should be considered as unimportant (see below).
6. DT: the di/trioctahedral substitution ($\square^{VI}Al^{VI}Al^{VI} = 3(Fe^{2+}, Mg)^{VI}$), which is responsible for an excess of octahedral content above the ideal value of Al-celadonite and muscovite (2 a.p.f.u.). This substitution leads to intermediate compositions between the muscovite–Al-celadonite binary and biotite end members ($K(Mg, Fe^{2+})_3(Si_3AlO_{10})(OH)_2$.

As outlined by Guidotti and Sassi (1998b), various problems are encountered during standard EMPA of KWM, among which the most important are the inability to determine Fe^{3+} and the nature of interlayer vacancies. Any attempt to use EMPA analyses of natural KWM for geothermobarometry should therefore first address the question of substitutions (4) and (5).

The pyrophyllitic substitution

This substitution is well known in low-grade, low-pressure environments where Si-rich and interlayer-deficient,

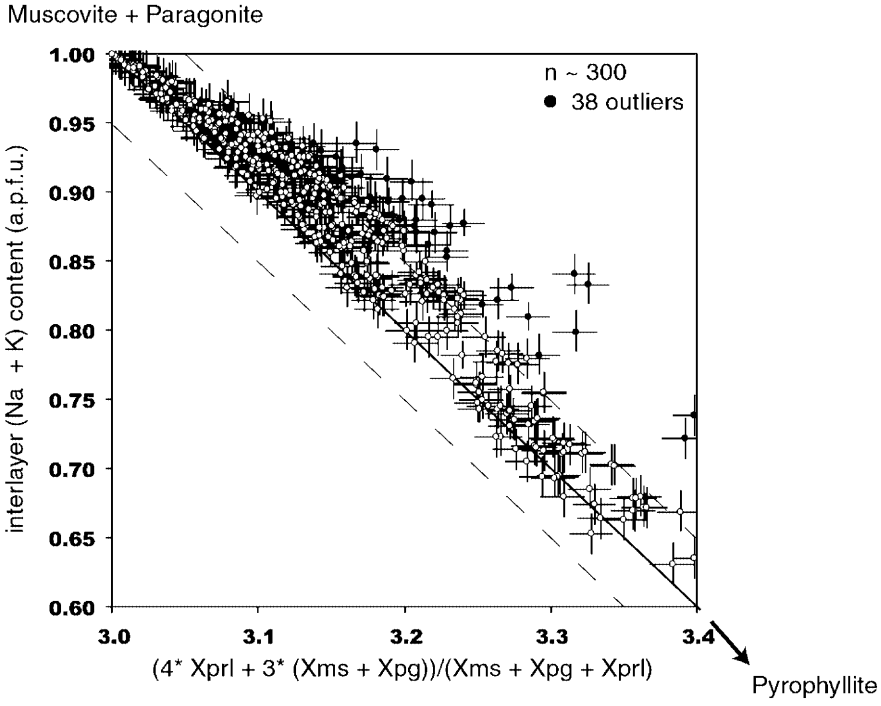

Fig. 1. KWM interfolial cation occupancy (Na + K a.p.f.u.) versus KWM Si content projected on the (Ms + Pg)–Prl binary. The Si content is recalculated from the end-member decomposition, considering only the muscovite, the paragonite and the pyrophyllite end members: $Si = (4\times X_{Prl} + 3\times(X_{Ms} + X_{Pg}))/(X_{Pg} + X_{Ms} + X_{Prl})$. A chemical analysis resulting from a true pyrophyllitic substitution should lie on the *continuous line*, or at least within the *dashed lines* which account for microprobe errors (2σ value). *Open circles* represent natural data from Table 5 (with 1σ standard deviation) whose composition can be explained by the pyrophyllitic exchange. *Closed circles* represent outliers (~12%) whose composition may result from substitutions not considered in this study and/or contamination by other minerals like quartz

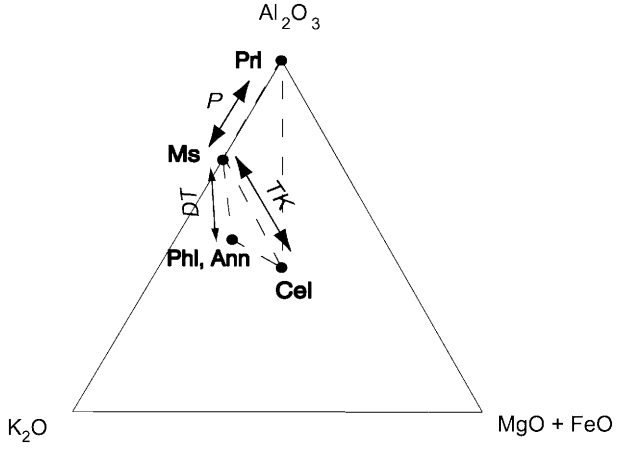

Fig. 2. Relevant substitutions responsible for the compositional variability of white micas represented in a Al–K–(Fe + Mg) ternary diagram. The composition of white mica can be expressed as a combination of Al-(Fe + Mg)-celadonite (*Cel* $Si_4AlMgKO_{10}(OH)_2$), muscovite (*Ms* $Si_3Al_2KO_{10}(OH)_2$), pyrophyllite (*Prl* $Si_4Al_2O_{10}(OH)_2$) and trioctaedral K micas, such as phlogopite and annite (*Phl* $Si_3AlFe_3KO_{10}(OH)_2$; *Ann* $Si_3AlFe_3KO_{10}(OH)_2$)

illitic KWM crystallize (Rieder et al. 1998; Frey and Robinson 1999). In metamorphic rocks, too, silica-rich and alkali-deficient KWM compositions were reported by Wang and Banno (1987), Bousquet (1998), Vidal and Parra (2000) and Agard et al. (2001). In these studies, the observed correlation between the Si, (Fe + Mg) and vacancy contents cannot be explained by the substitutions of K^+ by H_3O^+, NH_4^+ or H_2O, but rather by the incorporation of a pyrophyllite component (Table 2).

The existence of a pyrophyllite component in KWM is also suggested by Fig. 1, where most of the ca. 300 analyses plot on the muscovite/paragonite–pyrophyllite binary (within microprobe errors) and show a trend towards pyrophyllite. This indicates that the excess of silica (which was recalculated after taking into account the paragonite, pyrophyllite and muscovite parts; Fig. 1), compared to the ideal value of 3 a.p.f.u. muscovite, does not result from the TK substitution (Al-celadonite content) alone.

What remains unknown is whether this pyrophyllite component corresponds to a mechanical mixture or to a solid-solution phase. The TEM observations of Jiang et al. (1990) indicate that phyllosilicates of illite composition (as seen by EMPA) crystallizing in LT and LP pyrophyllite- and muscovite-bearing metapelites are actually a mechanical mixture of pyrophyllite and muscovite. From these observations, Jiang et al. (1990, 1992) concluded that illite is metastable with respect to pyrophyllite and muscovite. This conclusion is questioned by other TEM investigations of low-temperature samples. For example, Aja et al. (1991a, 1991b), Aja and Rosenberg (1992), Yates and Rosenberg (1993, 1996), and Aja (1995) claimed that compositions which cannot be taken for a mechanical mixture of pyrophyllite and muscovite (hence, a single illitic phase) formed within preexisting muscovite.

Table 2. Influences of alkali loss or the assumption $Fe_{total} = Fe^{2+}$ on KWM structural formulae, for three chemical analyses of KWM

Phengite analysis calculated on 11 oxygens									
Number	1[a]			2			3		
	Max. Fe^{3+}	All Fe^{2+}	10% alkali loss	Max. Fe^{3+}	All Fe^{2+}	10% alkali loss	Max. Fe^{3+}	All Fe^{2+}	10% alkali loss
SiO_2	48.050	48.050	48.050	50.511	50.511	50.511	49.796	49.796	49.796
TiO_2	0.060	0.060	0.060	0.203	0.203	0.203	0.205	0.205	0.205
Al_2O_3	33.820	33.820	33.820	26.204	26.204	26.204	26.016	26.016	26.016
FeO total	3.060	3.060	3.060	3.199	3.199	3.199	3.786	3.786	3.786
MnO	0.030	0.030	0.030	0.025	0.025	0.025	0.000	0.000	0.000
MgO	1.010	1.010	1.010	2.721	2.721	2.721	2.328	2.328	2.328
CaO	0.090	0.090	0.090	0.069	0.069	0.069	0.000	0.000	0.000
Na_2O	0.580	0.580	0.580	0.359	0.359	0.359	0.217	0.217	0.217
K_2O	9.250	9.250	8.325	10.117	10.117	9.105	10.350	10.350	8.733
F	0.000	0.000	0.000	0.000	0.000	0.000	0.000	0.000	0.000
Cl	0.000	0.000	0.000	0.000	0.000	0.000	0.000	0.000	0.000
Total	94.660	94.660	94.660	96.350	96.350	96.350	95.360	95.360	95.360
Si	3.148	3.173	3.184	3.432	3.446	3.459	3.425	3.438	3.460
Ti	0.003	0.003	0.003	0.010	0.010	0.010	0.011	0.011	0.011
Al	2.612	2.632	2.641	2.098	2.107	2.115	2.109	2.117	2.130
Fe^{2+}	0.000	0.169	0.170	0.097	0.182	0.183	0.133	0.219	0.220
Fe^{3+}	*0.168*	*0.000*	*0.000*	*0.085*	*0.000*	*0.000*	*0.084*	*0.000*	*0.000*
Mn	0.002	0.002	0.002	0.001	0.001	0.001	0.000	0.000	0.000
Mg	0.099	0.099	0.100	0.276	0.277	0.278	0.239	0.240	0.241
Ca	0.006	0.006	0.006	0.005	0.005	0.005	0.000	0.000	0.000
Na	0.074	0.074	0.075	0.047	0.047	0.048	0.029	0.029	0.029
K	0.773	0.779	0.704	0.877	0.880	0.795	0.908	0.911	0.774
F	0.000	0.000	0.000	0.000	0.000	0.000	0.000	0.000	0.000
Cl	0.000	0.000	0.000	0.000	0.000	0.000	0.000	0.000	0.000
Total	6.884	6.937	6.883	6.929	6.956	6.896	6.937	6.964	6.866
Si	3.148	3.173	3.184	3.432	3.446	3.459	3.425	3.438	3.460
Ti	0.003	0.003	0.003	0.010	0.010	0.010	0.011	0.011	0.011
Al(IV)	0.849	0.824	0.813	0.557	0.544	0.530	0.565	0.552	0.529
Al(VI)	1.763	1.807	1.828	1.541	1.563	1.585	1.544	1.565	1.601
Mg(M2)	0.068	0.072	0.064	0.277	0.264	0.250	0.239	0.228	0.209
Fe(M2)	0.000	0.118	0.105	0.097	0.174	0.165	0.133	0.208	0.190
Fe^{3+} (M2)	*0.168*	*0.000*	*0.000*	*0.085*	*0.000*	*0.000*	*0.084*	*0.000*	*0.000*
Mn(M2)	0.002	0.002	0.002	0.001	0.001	0.001	0.000	0.000	0.000
Mg(M1)	0.031	0.028	0.036	0.000	0.013	0.028	0.000	0.012	0.033
Fe(M1)	0.000	0.051	0.065	0.000	0.009	0.018	0.000	0.011	0.030
v(M1)	0.969	0.921	0.899	1.000	0.978	0.954	1.000	0.977	0.938
K(A)	0.773	0.779	0.704	0.877	0.880	0.795	0.908	0.911	0.774
Na(A)	0.074	0.074	0.075	0.047	0.047	0.048	0.029	0.029	0.029
v(A)	0.153	0.147	0.222	0.076	0.072	0.157	0.063	0.060	0.197
Fe^{3+} Musc	0.084	0.000	0.000	0.042	0.000	0.000	0.042	0.000	0.000
Prl	0.153	0.147	0.222	0.076	0.072	0.157	0.063	0.060	0.197
Phl	0.000	0.048	0.062	0.000	0.009	0.019	0.000	0.011	0.030
Ann	0.031	0.029	0.037	0.000	0.014	0.029	0.000	0.012	0.033
Pg	0.074	0.074	0.075	0.047	0.047	0.048	0.029	0.029	0.029
Fe-ACel	0.000	0.024	–0.016	0.097	0.155	0.127	0.133	0.185	0.131
Mg-ACel	0.006	0.013	–0.011	0.277	0.236	0.193	0.239	0.203	0.143
Ms	0.660	0.673	0.640	0.468	0.473	0.435	0.494	0.500	0.438
Total	1.008	1.008	1.008	1.007	1.007	1.007	1.000	1.000	1.000
Prl criterion	0.020	0.017	0.015	0.053	0.050	0.088	0.045	0.042	0.100
Tsch. criterion	0.003	0.021	–0.011	0.067	0.058	0.101	0.058	0.049	0.111
δSi	–0.031	–0.032	–0.032	–0.029	–0.029	–0.029	0.000	0.000	0.000
δAl^{VI}	–0.017	–0.017	–0.017	–0.014	–0.014	–0.014	0.000	0.000	0.000
$\delta(Mg + Fe^{2+})$	0.000	0.000	0.000	0.000	–0.001	–0.001	0.000	0.000	0.000
δK	–0.008	–0.008	–0.008	–0.007	–0.007	–0.007	0.000	0.000	0.000

[a]For each analysis, we show the EMP analysis, the structural formulae calculated on 11 oxygens, the cation distribution for the solid-solution model used in this study (see Table 3), the end-member decomposition, the exchange criteria for the Tschermak and the pyrophyllite vectors (see Appendix), and the scatter (δ) between the real cation content and the content recalculated from the end-member decomposition for Si, Al^{IV}, (Fe + Mg) and K. In order for the chemical analysis to be a linear combination of the end members, each end-member proportion must be positive and the total must be equal to one (within the uncertainty due to EMP analysis: ± 0.025). Similarly, the δ must be lower than 0.05 (value from microprobe uncertainties). If the Si content results from the Tschermak and pyrophyllitic vectors only, the Prl and Tsch. exchange criteria will be verified and the values lower than 0.060 and 0.070, respectively (see Appendix). For each analysis, we report the effect of the Fe^{3+} content in the first column, and the effect of the alkali loss in the third column. The second column corresponds to structural formulae assuming all iron is Fe^{2+}

These contrasting results suggest that TEM investigations may not be sufficient to solve the question of illite metastability and the existence of the pyrophyllite substitution at low T and P. Nevertheless, the correlation between the extent of the pyrophyllite substitution and P–T conditions (in low-T blueschist and greenschist facies environments; Wang and Banno 1987; Leoni et al. 1996, 1998; Vidal and Parra 2000; Agard et al. 2001; Trotet et al. 2001a, 2001b) seems more difficult to explain if pyrophyllite is a mechanical phase rather than a phase component (solid-solution end member). Consequently, in this study we will attribute the interfolial deficiency to the P substitution.

The ferrimuscovite substitution

The distinction between Fe^{2+} and Fe^{3+} is sometimes made by plotting the EMP data in Si–Al_{total} diagrams (Frey et al. 1988; Dalla Torre et al. 1996). Unfortunately, this plot is ambiguous when dealing with KWM containing a significant proportion of pyrophyllite and/or trioctahedral components. In fact, the incorporation of pyrophyllite leads to compositions plotting above the Al-celadonite–muscovite line, whereas the incorporation of ferrimuscovite and trioctahedral mica leads to compositions plotting below this line. Guidotti and Yates (1994) designed a method to broadly estimate the Fe^{3+} content of KWM, based on the opaque phase mineralogy. However, in the absence of direct measurement, it is impossible to estimate precisely the Fe^{3+} content from EMPA, and KWM are generally calculated assuming that $Fe_{total} = Fe^{2+}$. For Mg-rich natural KWM used in the present study, this common assumption has an influence on the calculated proportions and activities of the Fe-bearing end members (i.e., Fe-Al-celadonite, ferrimuscovite and annite) but almost none on their sum as well as on the atom distribution at the T2, M1, M2 and A sites, as seen from Table 2 (except for the Fe^{2+} content). This is mainly due to the large dilution of Fe^{3+} in these KWM. Therefore, whatever the assumptions regarding the oxidation state of iron, the activities of Mg-Al-celadonite, muscovite, pyrophyllite and paragonite in KWM, and the P–T estimates involving these end members are almost unchanged (Vidal and Parra 2000). On the basis of these observations, KWM structural formulae are calculated in the following, assuming that $Fe_{total} = Fe^{2+}$.

KWM solution model

Cation ordering and site distribution

The crystal structure of potassic white micas (KWM) is illustrated in Fig. 3. The basic layered T–O–T structure consists of a layer of octahedrally coordinated cations (Al, Fe, Mg) and two identical (Si, Al)O_3(OH) tetrahedral layers (Bailey 1975, 1984a, 1984b). Twelve coordinated interlayer cations (K, Na, etc.) are located between two T–O–T layers. Six distinct sites can be recognized:

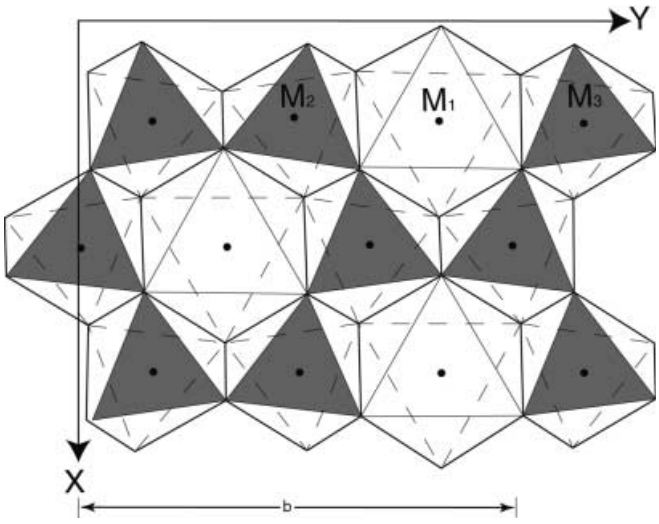

Fig. 3. Simplified sketch of the KWM crystal structure, illustrating the relative sizes of the M2 and M3 octahedral sites (*shaded*) and the vacant M1 site in 2M1-muscovite (Bailey 1984a)

two tetrahedral $(T1)_2$ and $(T2)_2$, three octahedral (M1) (M2) and (M3), and one interlayer A site.

The distribution of cations among the different sites is constrained by the following observations.

- Tetrahedral ordering is favored in the 3T structures, for phengitic compositions, and for $Si:Al^{IV}$ ratios near 1:1 (Bailey 1984a). For the other polytypes, refinements did not lead to the detection of any substantial degree of tetrahedral ordering in micas (see Bailey 1984a for more details). However, Haselton et al. (1995) claimed that comparison of the entropy of muscovite derived from heat capacity and heat content measurements suggests that the distribution of Al and Si in tetrahedral sites of 2M1 muscovite is nearly ordered. This indicates short-range Al/Si ordering, at least to the extent of obeying the Al-avoidance rule. In the following we assume a partial Si/Al ordering with T1 filled by Si only.
- Octahedral cation ordering occurs between cations of different sizes and charges (see Table 5 of Bailey 1984a). In particular, Al^{VI} shows a strong preference for M2 and M3 sites, whereas the vacancies and the excess of Fe + Mg cations resulting from the di/tri-octahedral substitution are primarily located in the larger M1 octahedrons (see Table 5 of Bailey 1984a).

The cation site distribution model used here, which stems from the above constraints, is given in Table 3. This model does not differentiate the M2 and M3 sites of similar sizes (collectively referred to as the M2 site of multiplicity 2).

Thermodynamic formulation and relevant thermodynamic properties

The formalism used in this study to calculate the end-member, standard-state thermodynamic properties and

Table 3. Cation distribution for the different end members in the four sites of the K white mica (KWM) solid solution

End member	T2(2)	M2(2)	M1(1)	A(1)
Muscovite	SiAl	AlAl	❑[a]	K
Paragonite	SiAl	AlAl	❑	Na
Mg-Al-celadonite	SiSi	AlMg	❑	K
Fe^{2+}-Al-celadonite	SiSi	$AlFe^{2+}$	❑	K
Pyrophyllite	SiSi	AlAl	❑	*v*[b]
Annite	SiAl	$Fe^{2+}Fe^{2+}$	Fe^{2+}	K
Phlogopite	SiAl	MgMg	Mg	K

[a] ❑ represents the M1-site vacancy
[b] *v* represents the interlayer vacancy

the mixing parameters is similar to that described by Berman and Brown (1984) and Mäder et al. (1994), and used by Vidal et al. (2001) for chlorites.

For any balanced chemical reaction among *j* species, the equilibrium condition is

$$0 = \sum_j v_j \Delta_a G_j^{P,T} + RT \ln K \quad (1)$$

where v_j is the stoichiometric reaction coefficient, $\Delta_a G^{P,T}$ is the change in the apparent Gibbs free energy of formation, and K is the equilibrium constant which can be written as

$$K = \left[\prod_j (a\gamma_m)_j^{v_j} \right]_{equilibrium} \quad (2)$$

where a_{ideal} is the ideal (configurational) part of the activity, and γ_m is the activity coefficient, accounting for non-ideal contributions to the activity. For the symmetric interactions assumed at the octahedral sites T2, M2 and M1, γ_m is computed from the following equation, which is a simple extension of the classic Wohl's equation (Cheng and Guanguly 1994) but dropping the ternary interactions terms:

$$n_s.R.T.\ln\gamma_m = \sum W_{ij}.x_i.x_j.\left[\frac{Q_m.r_m}{x_m.n_s} - 1\right] \quad (3a)$$

where n_s is the multiplicity of site *s*, r_m the number of cations *m* at each site, x_m the mole fraction of cation *m* at site *s*, W_{ij} the Margules parameters ($W_{ij} = W^H_{ij} + W^S_{ij} \times T + W^V_{ij} \times P$), and Q_m the number of *i*, *j* subscripts which are equal to *m*.

For the asymmetric interactions assumed at the interlayer site A^{XII}, γ_m is computed from

$$n_s.R.T.\ln\gamma_m = \sum W_{ijk}.x_i.x_j.x_k.\left[\frac{Q_m}{x_m} - 2\right] \quad (3b)$$

Equation (1) can be rearranged to compute the unknown thermodynamic parameters for known mineral compositions and P–T conditions. A four-site mixing model and ideal intersite interaction have been adopted to model chemical exchange in KWM (Tables 3 and 4).

The input data discussed below are insufficient to derive a unique estimate of each solution parameter for all possible interactions at each site (Table 3). For this reason and by analogy to the chlorite model derived by Vidal et al. (2001), intersite interactions, W_{Al-Si} at T2 and W_{Fe-Mg} at M2 and M1 were assumed to be zero (ideal behavior of same ionic radius cations). For the symmetric interaction model between cations at M2 used in this study, $C_{Al-Fe-Mg}$ at M2 is equal to zero (Cheng and Ganguly 1994). At site A, the components have different energetic properties, which precludes to estimate the C_{K-Na-v} parameter as suggested by Cheng and Ganguly (1994). C_{K-Na-v} was assumed to be zero. The remaining adjustable Margules parameters are therefore W_{Al-Mg} and W_{Al-Fe} at M2, $W_{□-Mg}$ and $W_{□-Fe}$ at M3, and W_{Na-v}, W_{v-Na}, W_{K-v}, W_{v-K}, W_{K-Na} and W_{Na-K} at A^{XII}. Moreover, since the trioctahedral content is largely dependent on the Fe^{3+} content, we assumed that $W_{□-Mg} = W_{□-Fe} = 0$ at M1. As a consequence, the DT substitution is not calibrated, and the annite and phlogopite end members should not be used to estimate pressure and temperature.

The standard-state properties of muscovite, paragonite, and pyrophyllite were taken from the database of Berman (1988). The remaining adjustable standard-state properties are the enthalpy, molar volume and third-low entropy of Mg- and Fe-Al-celadonite.

Input data

Thermodynamic properties are primarily constrained with available experimental data, which are then adjusted and extrapolated outside the P-T-composition experimental range using selected natural data.

Experimental constraints

The available experimental data provide constraints on Mg–Al, Fe–Al, Fe–Mg and K–Na interactions. The

Table 4. Ideal part of the activity of the KWM end members, calculated for a multisite ionic model

End member	Ideal part of activity[a]
Muscovite	$a_{Ms} = ((Si-2)/2)\bullet(Al^{IV}/2)\bullet 4\bullet(Al^{VI}/2)^2\bullet❑\bullet K$
Paragonite	$a_{Pg} = ((Si-2)/2)\bullet(Al^{IV}/2)\bullet 4\bullet(Al^{VI}/2)^2\bullet❑\bullet Na$
Mg-Al-celadonite	$a_{Mg\text{-}Al\text{-}cel} = ((Si-2)/2)^2\bullet(Al^{VI}/2)\bullet(Mg^{M2}/2)\bullet 4\bullet❑\bullet K$
Fe^{2+}-Al-celadonite	$a_{Fe^{2+}\text{-}Al\text{-}cel} = ((Si-2)/2)^2\bullet(Al^{VI}/2)\bullet(Fe^{M2}/2)\bullet 4\bullet❑\bullet K$
Pyrophyllite	$a_{Prl} = ((Si-2)/2)^2\bullet(Al^{VI}/2)^2\bullet❑\bullet v$
Annite	$a_{Ann} = ((Si-2)/2)\bullet(Al^{IV}/2)\bullet 4\bullet(Fe^{M2}/2)^2\bullet Fe^{M1}\bullet K$
Phlogopite	$a_{Phl} = ((Si-2)/2)\bullet(Al^{IV}/2)\bullet 4\bullet(Mg^{M2}/2)^2\bullet Mg^{M1}\bullet K$

[a] ❑ represents the M1-site vacancy
[b] *v* represents the interlayer vacancy

octahedral interactions are constrained by data in the KMASH, KFASH, and KFMASH systems, whereas the K–Na interaction is constrained by the data in the KNASH system.

KMASH and KFASH systems

Massonne and Schreyer (1986, 1987, 1989), Massonne (1995) and Massonne and Szpurka (1997) reported numerous experimental data in both systems dealing with the P-T-composition dependency of KWM in equilibrium with either K-feldspar + phlogopite + quartz (FkPQ), pyrope + kyanite + quartz/coesite (PyKQ/C), talc + kyanite + quartz/coesite (TaKQ/C), or almandine + kyanite + quartz/coesite (AKQ/C), respectively. The experiments involving talc were not included in the input data set because of the uncertainties on its standard-state properties and activity-composition relationship. For the AKQ/C equilibria, run GV57 was not considered because the octahedral occupancy was not determined. Run GV60 was also omitted because it led to the crystallization of an Md polytype, whereas 2M1 polytypes crystallized in all the other runs. For the remaining data, the activity of all phases except KWM and phlogopite were assumed to be unity. The activity of phlogopite estimated by Massonne and Szpurka (1997) was allowed to vary within ± 0.02. The uncertainties estimated by Massonne and Schreyer (1987) and Massonne and Szpurka (1997) on the KWM Si content ($\sigma(\mathrm{Si})_{T1+T2} = \pm 0.04$ a.p.f.u.) and octahedral occupancy ($\sigma(\mathrm{Oct.})_{M2+M3} = \pm 0.015$ a.p.f.u) were enlarged to ± 0.05 and ± 0.02, respectively. These latter values are believed to be more realistic and account for the differences observed between the Si contents derived from XRD and EMPA (e.g., for the runs V934 and V940). As the Al:Mg ratio at the M2 site results from the TK and DT substitutions, uncertainties on Mg and Al contents at M2 correspond to $\sigma(\mathrm{Al})_{M2} = \sigma(\mathrm{Mg})_{M2} = \sigma(\mathrm{Si})_{T1+T2} + 2\times\sigma(\mathrm{Oct.})_{M2+M3} = \pm 0.09$. Following Massonne and Szpurka (1997), a 2σ error of $\pm 2\%$ on temperature was assumed for the buffered experiments ($\pm 1\%$ for other experiments), and a 2σ error of $\pm 1\%$ on pressure.

KFMASH system

Krogh and Raheim (1978) and Green and Hellman (1982) have investigated the evolution of the Fe^{2+}–Mg distribution between garnets and KWM. Green and Hellman (1982) studied the Fe–Mg exchange reaction between the two minerals by reacting natural phengite and garnet in the presence of quartz at temperatures between 800 and 1,000 °C and water pressures between 20 and 35 kbar. We only used experiments which contain "true" phengite (runs with KWM octahedral occupancy close to 2.5 were omitted), and for which EMPA are available. Krogh and Raheim (1978) used a set of three experiments combined with data for natural rocks to calibrate three Fe–Mg exchange geothermometers depending on bulk-rock composition. We used the experimental runs which were carried out at 30 kbar and temperatures between 700 and 1,000 °C. In both cases, we assumed 2σ uncertainties of $\pm 1{,}000$ bar and ± 25 °C on pressure and temperature, respectively, and a 2σ uncertainty of 5% was introduced on $\ln K_D = \ln((\mathrm{Fe/Mg})_{Gt}/(\mathrm{Fe/Mg})_{Pheng})$ to account for the uncertainties on the compositions given by the authors.

KNASH system

Major inconsistencies exist among the different sets of experimental data dealing with the location and shape of the muscovite–paragonite solvus (Eugster and Yoder 1955; Iiyama 1964; Eugster et al. 1972; Blencoe 1974; Chatterjee and Froese 1975; Blencoe 1977; Chatterjee and Flux 1986; Roux and Hovis 1996). Blencoe et al. (1994) suggested that the thermodynamic model of Chatterjee and Froese (1975; constrained by experiments from Eugster et al. 1972) best fits natural data. For this reason, we preferentially used the experimental results of Eugster et al. (1972) to constrain the W_{K-Na} and W_{Na-K} Margules parameters. These experimental results were combined with all the available volume measurements on the paragonite–muscovite binary (Burnham and Radoslovich 1964; Zen et al. 1964; Guven 1971; Rothbauer 1971; Eugster et al. 1972; Chatterjee 1974; Chatterjee and Johannes 1974; Flux and Chatterjee 1986; Roux and Hovis 1996).

Natural data

Selection of the analyses

About 250 analyses of KWM from the literature, from various rock compositions and parageneses formed under contrasting P–T conditions (Table 5) were selected according to the following criteria.

1. They span a range of P–T conditions large enough to permit extrapolation of the solid-solution model outside the experimental P–T range.
2. Mineral assemblages, or the geological context, provide independent P–T estimates.
3. Textural and chemical evidences testify to equilibrium between the relevant minerals (lack of reaction features). When different mineral generations appeared to coexist in the same thin section, we selected the analyses likely to correspond to the peak of pressure, that is, analyses showing the largest Al-celadonite content. When enough analyses were available, we averaged the compositions representative of a population of at least three analyses in the same thin-section area. If zoning was evidenced (as is sometimes the case in KWM, Dempster 1992), we considered rim analyses only.
4. In order to limit the possibility for KWM to contain Fe^{3+}, we preferentially used carboneous-bearing samples. This guarantees at least a low oxygen fugacity,

Table 5. Natural data set used to calibrate the thermodynamic and excess properties of the KWM. P_{orig}–T_{orig} Original P–T estimates given by the authors, P_{ref}–T_{ref} P and T which were used as references in the optimization procedure (see below)

P–T domains[a]	Locality	Host rock	Mineral assemblages	Reference	P_{orig}–T_{orig} (kbar/°C)	P_{ref}–T_{ref} (kbar/°C)
1: HP–LT	Engadine Window (Alps, Switzerland)	Metapelites	Carpholite–chlorite–KWM–paragonite–quartz (± pyrophyllite, ± kaolinite)	Bousquet et al. (1998)	10–14, 300–400	A, B
	Schistes Lustrés (Western Alps)	Metapelites	Chlorite–KWM–carpholite–quartz	Agard (1999)	10–20, 350–400	A, B
	Northwest Turkey	Blueschists	Chlorite–KWM ± chloritoid–paragonite ± jadeite–quartz	Okay and Kelley (1994)	18–22, 410–480	B
	External Hellenides (Greece)	Metapelites	KWM–garnet–chloritoid–quartz	Theye and Seidel (1991)	13–21, 420–480	A
2: HP–HT	Dora Maira (Western Alps)	Metapelites	KWM–garnet–biotite–quartz	Hirajima and Campagnoni (1993)	15–27, 650–750	A
	Santiago schists (NW Iberian massif, Spain)	Metapelites	KWM–garnet–chlorite–quartz	Arenas et al. (1995)	6.5–15, 480–530	B
	Grand Paradis (Alps, France)	Metapelites	Chlorite–KWM–chloritoid–quartz (± talc, ± garnet)	Chopin (1985)	10–20, 450–600	B
	Syros Island (Greece)	Sodic schists	Chlorite–KWM ± garnet ± glaucophane ± albite ± paragonite ± jadeite–quartz	Trotet et al. (2001a, 2001b)	10–19, 450–600	A, B
	Adula Nappe (Central Alps)	Metapelites	KWM–plagioclase–garnet–quartz	Heinrich (1982, 1986)	10–25, 450–700	A
	Henan Province (central China)	Eclogites	KWM–garnet–paragonite–glaucophane–Na and Ca pyroxenes–quartz	Zhang and Liou (1994)	20–30, 500–650	A
	Escuador (Andes)	Pelitic schists	KWM–garnet–paragonite ± jadeite–quartz	Feininger (1980)	10–16, 560–600	A
	Sambagawa Belt (Shikuko Island, Japan)	Sodic schists	KWM–chlorite–paragonite–albite–quartz	This study	10–12, 510–580	A
	Tinos Island (Greece)	Sodic schists	Chlorite–KWM–paragonite–albite–quartz (± epidote)	This study	10–15, 500–550	A
	Meliata unit (West Carpathians, Slovakia)	Blueschists	Chlorite–KWM–Ca-amphibole–quartz	Faryad (1995)	7–12, 450–650	A
3: LP–HT	Mt. Moosilauke (New Hampshire, USA)	Pelitic schists	Quartz–KWM–biotite–plagioclase–garnet–Al_2O_3 (sillimanite, andalusite or kyanite)	Hodges and Spear (1982)	2.5–5, 450–600	C

	West central Massachussets (USA)	Pelitic schists	Quartz–KWM–biotite–plagioclase–garnet–Al_2O_3 (sillimanite, andalusite or kyanite)	Tracy (1978)	2.5–4.5, 550–750	C
	Shuswap metamorphic core complex (British Columbia)	Pelitic schists	Quartz–KWM–biotite–plagioclase–garnet–Al_2O_3 (sillimanite, andalusite or kyanite)	Pigage (1976, 1982)	4–6, 520–580	C
	Quesnel Lake (Canadian Cordillera)	Pelitic schists	Quartz–KWM–biotite–plagioclase–garnet–Al_2O_3 (sillimanite, andalusite or kyanite)	Fletcher and Greenwood (1978)	5.5–8.5, 650–710	C
	File Lake Area (Manitoba)	Pelitic schists	Quartz–KWM–biotite–plagioclase–garnet–Al_2O_3 (sillimanite, andalusite or kyanite)	Gordon et al. (1991)	2–4, 500–580	C
	South Royalton and Gassets (Vermont, USA)	Metapelites	Chlorite–KWM–garnet–plagioclase–biotite–quartz– ± paragonite	Giaramita and Day (1991)	MP–HT	C
	Shangdan fault zone (China)	Metapelites	KWM–garnet–biotite–plagioclase–quartz	Nengao et al. (1993)	5–10, 500–600	C
	Southeast Tauern Window (Austria)	Metapelites	KWM–plagioclase–garnet–quartz	Droop (1985)	6–8, 560–610	A
4: LP–LT	Internal Liguride units (Northern Appennines, Italy)	Al-saturated metapelites	Chlorite–KWM–quartz	Leoni et al. (1998)	2–7, 160–350	A
	Tinos Island (Greece)	Sodic schists	Chlorite–KWM–paragonite–albite–quartz (± epidote)	This study	3–8, 350–450	A
	Verrucano metasediments (Northern Apennines, Italy)	Metapelites	Quartz–KWM–pyrophyllite ± sudoite ± chloritoid	Giorgetti et al. (1998)	7–10, 320–420	A
	Northern Pensylvania, Witwatersrand (South Africa)	Metapelites	KWM–pyrophyllite	Jiang et al. (1990)	< 5, 350	A
	Northern range (Trinidad, West Indies)	Metasediments	KWM–pyrophyllite–chlorite ± chloritoid–quartz	Frey et al. (1988)	2, 325	A
	Augusta (Maine, USA)	Sodic schists	KWM–feldspar	Ferry (1978, 1979, 1992)	3.5, 300–500	A

[a] 1, high-pressure/low-temperature domain; 2, high-pressure/high-temperature domain; 3, low-pressure/high-temperature domain; 4, low-pressure/low-temperature domain; A, original P–T estimates; B, Intersx P–T estimates; C, Intersx T estimates and Hoisch (1990) geobarometer P estimates

and consequently a low Fe^{3+} content in KWM (Guidotti and Yates 1994).
5. Quartz is in excess (or coesite for UHP assemblages).
6. In order to discard contaminated analyses, we only retained EMP analyses with an oxygen sum between 92 and 96 wt%, and showing less than 0.5 wt% ($TiO_2 + MnO + CaO$). Moreover, they are strictly a linear combination of the seven end members (Mg- and Fe-Al-celadonite, muscovite, annite, phlogopite, paragonite, muscovite and pyrophyllite) and satisfy a series of equalities (for further details, see Appendix). Only 250 analyses out of the initial set of 300 fulfilled these criteria (outliers in Figs. 1 and 4 were discarded).

Type of parageneses and P–T conditions of reference

The natural samples used to constrain thermodynamic data correspond to four different ranges of metamorphic peak (Table 5).

HP–LT conditions (T < 400–450 °C, P > 10–12 kbar)

Carpholite-bearing samples (carpholite + trioctahedral chlorite + quartz + KWM parageneses) were collected in the Schistes Lustrés unit, Western Alps (Agard et al. 2001) and in the Engadine Window (Bousquet 1998; Bousquet et al. 1998). In both data sets, various KWM generations with different compositions have been identified on the basis of microstructural criteria. The pressure and temperature conditions for assemblages involving chlorites containing more than 5% (Fe, Mg)-sudoite end member were recalculated using the carpholite–chlorite–quartz–water paragenesis, as indicated in Vidal et al. (2001). For chlorite with less than 5% (Fe, Mg)-sudoite end member, it is not possible to calculate confident pressure and temperature simultaneously because the uncertainty on the activity of sudoite in chlorite is too large. In this case, we used as a reference the original P–T conditions given by the authors. The three other parageneses (chlorite + KWM + paragonite + jadeite + quartz, chlorite + KWM + glaucophane + paragonite + quartz, and chlorite + KWM + chloritoid + quartz) correspond to samples from northwest Turkey (Okay and Kelley 1994), the external Hellennides (Theye and Seidel 1991), and the Schistes Lustrés unit, Western Alps (Agard et al. 2001). Pressure and temperature conditions for the chloritoid-bearing assemblages involving chlorite were re-estimated with the TWQ software (Berman 1991) implemented with thermodynamic data for Fe-chloritoid (Vidal et al. 1994), Mg-chloritoid (Vidal et al. 1999), carpholite and sudoite (Vidal et al. 1992), and the solid-solution model published for chlorite by Vidal et al. (2001). The new temperature estimates for the Chl-Cld-bearing samples are close (±20 °C) to those estimated with the empirical Fe–Mg exchange thermometer of Vidal et al. (1999). For the two other parageneses, the original P–T values given by the authors were taken as a reference.

HP–HT conditions (T > 400–450 °C, P > 10–12 kbar)

Al-celadonite-rich phengites were shown to be one of the most likely mineral remnants of peak pressure conditions in high-pressure parageneses affected by exhumation-related retrogression (e.g., Frey et al. 1983). For this reason, they were used here to infer peak pressure estimates. Whenever possible, P–T conditions were re-estimated independently without considering the KWM (see Table 5). In other cases, we used the peak pressure conditions given by the authors. In addition to the data from the literature (Feininger 1980; Heinrich 1982; Chopin and Monié 1984; Arenas et al. 1995; Chopin 1985; Heinrich 1986; Hirajima and Campagnoni 1993; Zhang and Liou 1994; Trotet et al. 2001a, 2001b), we also considered unpublished data obtained from samples collected in the Cycladic blueschists (Tinos Island, Greece; Patriat 1996; Jolivet and Patriat 1999; Vidal and Parra 2000) and the Sambagawa Belt (Shikoku Island, Japan; Banno and Nakajima 1992; Enami et al. 1994). Samples from Tinos Island were collected in the lower Cycladic blueschist unit along a transect marked by an increasing degree of greenschist overprint from base to top, below the detachment zone with the upper ophiolitic unit (Jolivet and Patriat 1999; from Panormos to Isternia). The main interest of the Tinos samples is to provide a continuous variation of the KWM and chlorite compositions involved in the same parageneses (Chl–KWM–Gln or Ab–Pg–Qtz) from well-preserved blueschist to highly retrogressed, greenschist facies rocks. In some samples, Chl–KWM–Qtz parageneses involve chloritoid and/or garnet instead of Ab and Gln. Samples from the Sambagawa Belt were collected in the albite–biotite zone of the central part of Shikoku Island, along the Asemigawa River which crosscuts the metamorphic zonation. A similar observation is made for these samples, i.e., intensity of retrogression increases from the center of the Ab–Bt unit towards the upper garnet zone at the top of the tectonic pile and the oligoclase–biotite zone at the base (Radvanec et al. 1994).

For the samples containing Chl–KWM–Cld–Qtz or Chl–Gt–Phg–Qtz, P–T conditions were re-estimated without considering the KWM. For the others samples (Chl + KWM + Pg + Ab or Gln + Qtz), we used the P–T ranges given by the authors (Bröcker (1990) for Tinos Island samples, and Enami et al. (1994) for the Sambagawa Belt samples).

LP–HT conditions (T > 400–450 °C, P < 10–12 kbar)

All the parageneses considered here (Table 5) consist of KWM + Qtz + biotite + plagioclase + garnet ± chlorite ± aluminosilicates (except the data of Faryad 1995 where KWM coexist with amphiboles and Gt). Thermodynamic data and solid-solution properties for these minerals are included in the TWQ 2.01 software (amphibole: Mäder et al. 1994; biotite: McMullin et al. 1991; feldspar: Fuhrman and Lindsley 1988; garnet:

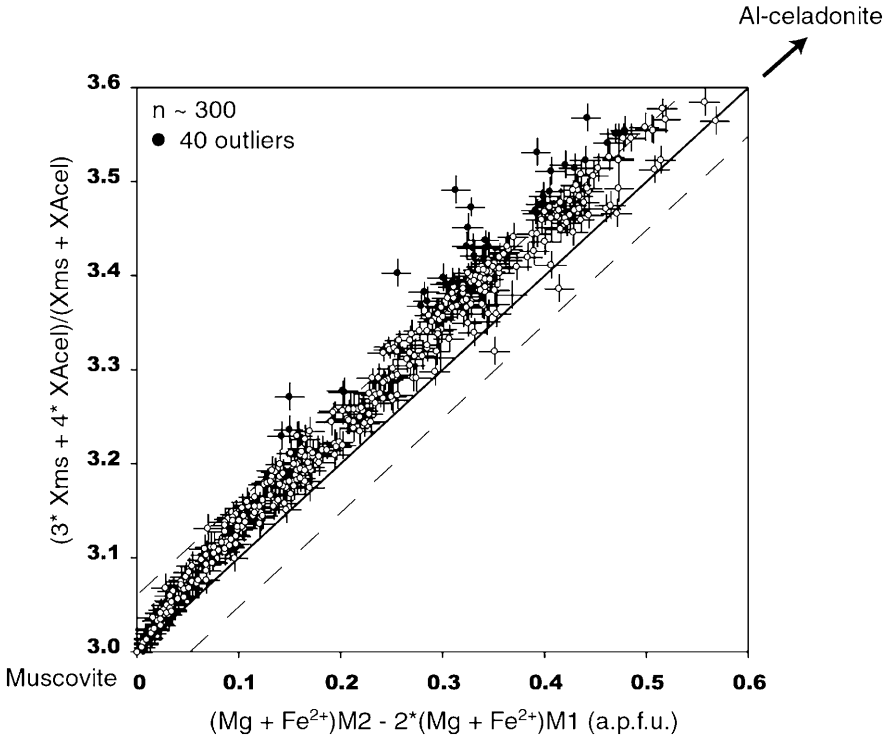

Fig. 4. KWM octahedral (Fe + Mg) occupancy (corrected for the DT substitution): (Mg + Fe)(M2)–2×(Mg + Fe)(M1), versus KWM Si content projected on the Ms–ACel binary. The Si content is recalculated from the end-member decomposition, considering only the muscovite and the Al-celadonite end members: $Si = (4\times X_{ACel} + 3\times X_{Ms})/(X_{Ms} + X_{ACel})$. A chemical analysis resulting from a true Tschermak substitution should lie on the *continuous line*, or at least within the *dashed lines* which account for microprobe errors (2σ value). *Open circles* represent natural data from Table 5 (with 1σ standard deviation) whose composition can be explained by the Tschermak exchange. *Closed circles* represent outliers (~12%) whose composition may result from substitutions not considered in this study and/or contamination by other minerals like quartz

Berman 1990). For the chlorite-bearing samples, the P–T conditions were re-estimated without considering the KWM. For samples lacking chlorite, temperature estimates are based on the biotite–garnet Fe–Mg equilibrium at the original pressure reported by Hoisch (1990). The reference P–T conditions obtained this way are consistent with the stability field of the aluminosilicates present in these parageneses (aluminosilicates were only used to check the validity of the new P–T estimates obtained with the thermodynamic data extracted in the present study).

LP–LT conditions (T < 400–450 °C, P < 10–12 kbar)

LP–LT parageneses are devoid of low-variance assemblages and the P–T conditions prevailing during the formation of KWM are difficult to assess and even questionable (Essene and Peacor 1995). The data of Leoni et al. (1996, 1998) were preferentially used because the authors document chemical correlations between the compositions of coexisting KWM and chlorite which are related to the evolution of the estimated P–T conditions (temperature determined from the illite crystallinity and pressure from the "b_0" parameter of illite as well as additional data from the literature). However, the KWM compositions of the Cravasco/Voltaggio and Mt. Figogna units (Leoni et al. 1996, 1998) are surprisingly similar to the KWM composition of the carpholite-bearing samples from the HP–LT domain (see above) in terms of pyrophyllitic and Tschermak contents, suggesting that the KWM of these units crystallized at higher pressure than that proposed by Leoni et al. (1996). Higher peak pressure conditions than reported by Leoni et al. (1998) for the Cravasco/Voltaggio unit is also suggested by the occurrence of blue amphibole in metabasites and carpholite in metapelites (B. Goffé and L. Martin, personal communication).

Calculation procedure

The unknown thermodynamic properties identified above (W^G_{Al-Mg}, W^G_{Al-Fe} at M2 , $W^G_{Na-\square}$, $W^G_{\square-Na}$, $W^G_{K-\square}$, $W^G_{\square-K}$, W^G_{Na-K}, and W^G_{K-Na} at A, as well as the standard-state properties of Mg- and Fe-Al-celadonite) were calculated using a step-by-step method similar to that adopted by Vidal et al. (2001) for chlorite. We started with a subset of the most constraining input data to estimate all the possible thermodynamic properties which were kept constant in the following steps. In the following step, we used another subset of less constraining data to calculate other thermodynamic properties, and so on until all the input data were used and all the thermodynamic properties were calculated. As discussed below, natural analyses were used so as to allow for the influence of each substitution to be identified independently.

Expansivity, compressibility and volume parameters of Al-celadonite

The expansivity and compressibility terms of Al-celadonite were assumed to be similar to that of muscovite. The Cp(T) functions for Mg-Al- and Fe-Al-celadonite were estimated according to Berman and Brown (1985), and their standard-state volumes as well as the excess volume functions along the muscovite–Mg-Al-celadonite and muscovite–Fe-Al-celadonite binaries were calculated from the volume-composition measurements reported by Massonne and Schreyer (1986), Massonne and Szpurka (1997) and Schmidt (1998) in the KMASH system, and Massonne and Szpurka (1997) in the KFASH system.

Results are shown in Fig. 5a, b and values are reported in Table 6. The standard-state molar volume of Mg-Al-celadonite estimated here is intermediate between those obtained by Holland and Powell (1998) and Massonne and Szpurka (1997), who could not consider the data of Schmidt (1998) at that time. As shown in Fig. 5b, the experimental constraints on V^0 of Fe-Al-celadonite are weak, partly because most of the data were obtained for a small range of composition. For this reason, V^0 of Fe-Al-celadonite was further constrained using natural data (see below). The resulting value is somewhat larger than that proposed by Holland and Powell (1998).

The volume-composition data were fitted with the function

$$Vx_{ms}.V^0_{ms} + x_{cel}.V^0_{cel} + V_{excess}$$

where

$$V_{excess} = x_{ms}.\left[x^{M2}_{Al}.x^{M2}_{Mg}.\left(\frac{1}{1.x^{M2}_{Al}} - 1\right).W^{V}_{(Al-Mg)_{M2}}\right] + x_{cel}.\left[x^{M2}_{Al}.x^{M2}_{Mg}.\left(\left(\frac{1}{2.x^{M2}_{Al}} - 1\right) + \left(\frac{1}{2.x^{M2}_{Mg}} - 1\right)\right).W^{V}_{(Al-Mg)_{M2}}\right]$$

which simplifies to the common expression

$$V_{excess} = x^{M2}_{Al}.x^{M2}_{Mg}.W_v^{(Al-Mg)_{M2}}$$

with

$$x_{ms} = x^{M2}_{Al} - x^{M2}_{Mg}$$

$$x_{cel} = 2.x^{M2}_{Mg}$$

Entropy, enthalpy of Mg-Al-celadonite and $W^G_{Al–Mg(P,\ T)}$

The entropy of Mg-Al-celadonite was calculated using the model of Holland (1989) and allowed to vary within ±2%. The standard-state properties of Mg-Al-celadonite as well as a preliminary, temperature-independent $W^G_{Al–Mg} = W^{G,\ 1\ bar}_{Al–Mg} + P \bullet W^V_{Al–Mg}$ function were calculated by mathematical programming using the experimental results along with the $W^V_{Al–Mg}$ calculated above. This

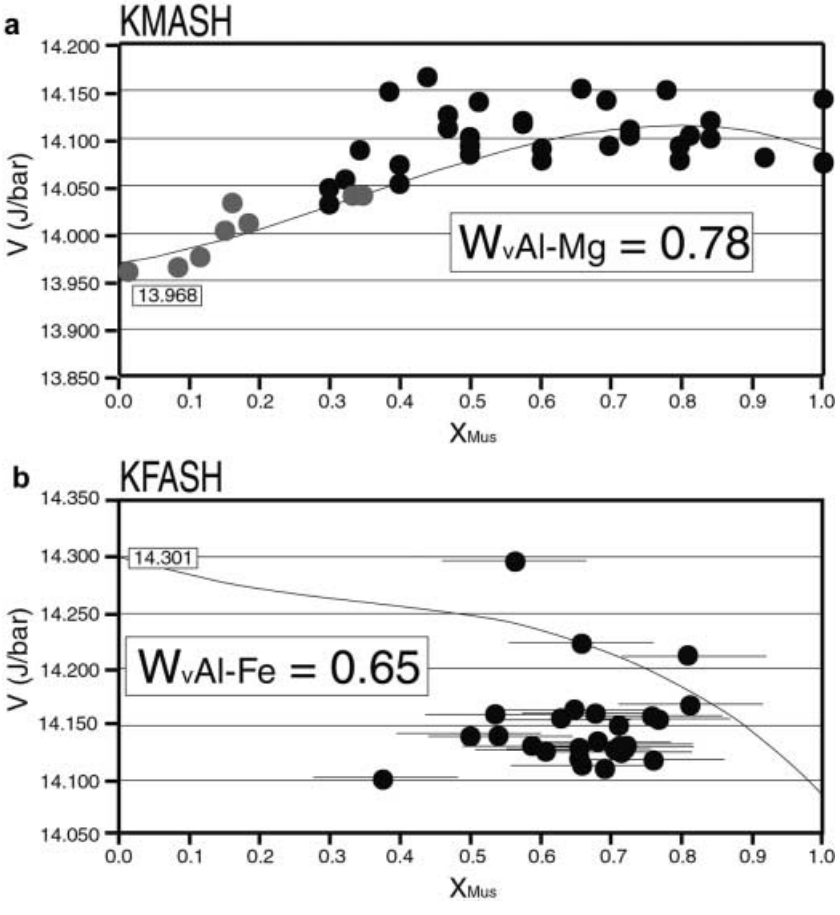

Fig. 5. **a** V^0 for the Al-Mg-celadonite end member and V for the Tschermak substitution in the KMASH system, resulting from a regression analysis on the experiments of Massonne and Szpurka (1997) and Schmidt (1998). The V^0 of muscovite is set to 14.087 J/bar to preserve the consistency with the data set of Berman (1988). **b** V^0 for Al-Fe-celadonite end member and V for the Tschermak substitution in the KFASH system, resulting from the optimization of the natural data set (Table 5) and the experiments of Massonne and Szpurka (1997). The V^0 of muscovite is set to 14.087 J/bar to preserve the consistency with the data set of Berman (1988)

Table 6. Thermodynamic properties of the Al-celadonite and Tschermak excess parameters in the KFASH and the KMASH systems

	Holland and Powell (1998)	Massonne and Szpurka (1997)	This study
KMASH			
H^0	–5,844,530.000	–5,832,415.000 ± 3,040.000	–5,834,736.700
S^0	287.000	288.527 ± 4.008	291.000
V^0	14.040	13.870 ± 0.027	13.968
Activity model	Ionic	Molecular	Ionic
	Ideal	Non-ideal	Non-ideal
		Asymmetric	Symetric
$W^H_{Al–Mg}$		0.000	–30,500.000
Mg–Al		0.000	–30,500.000
$W^S_{Al–Mg}$		58.598	15.000
Mg–Al		15.920	15.000
$W^V_{Al–Mg}$		0.735	0.780
Mg–Al		0.187	0.780
KFASH			
H^0	–5,497,340.000	–5,492,287.000 ± 6,267.000	–5,478,134.63
S^0	318.000	303.148 ± 6.827	330.170
V^0	14.250	13.962 ± 0.067	14.301
Activity model	Ionic	Molecular	Ionic
	Ideal	Non-ideal	Non-ideal
		Symmetric	Symmetric
$W^H_{Al–Fe}$		0.000	–5,500.000
Fe–Al		0.000	–5,500.000
$W^S_{Al–Fe}$		24.083	15.000
Fe–Al		24.083	15.000
$W^V_{Al–Mg}$		0.339	0.650
Fe–Al		0.339	0.650

preliminary W^G allowed to fit the experimental data fairly well but not the low-temperature natural data. The final standard-state properties of Mg-Al-celadonite as well as $W^H_{Al–Mg}$ and $W^S_{Al–Mg}$ were therefore adjusted by considering the carpholite-bearing samples, the chlorite–KWM LP–LT assemblages of Leoni et al. (1996, 1998), and the experimental constraints simultaneously. These natural data were preferentially considered because (1) they correspond to P–T conditions outside the range of experimental conditions, (2) they involve KWM with high Al-celadonite contents and high X_{Mg} which insure a negligible influence of the Fe–Al interactions on the Al-Mg-celadonite activity, (3) different generations of KWM have been clearly identified using microtextural criteria (Agard et al. 2001) and the corresponding P–T conditions can be calculated independently, (4) these natural data also involve chlorite, which allows one to estimate pressure conditions with the equilibrium Mg-Al-celadonite + Mg-amesite = muscovite + clinochlore. Since muscovite and Mg-Al-celadonite are on each side of the equilibrium with the same stoichiometric coefficients, the influences of the K–Na, K–*v* and Na–*v* interactions cancel out in the equilibrium constant. Moreover, the use of this equilibrium ensures consistency between the thermodynamic data of KWM and chlorite, and it is independent of the water activity.

$W^G_{Al–Fe(P,\ T)}$

A preliminary $W^G_{Al–Fe} = W^H_{Al–Fe} – T \bullet W^S_{Al–Fe} + P \bullet W^V_{Al–Fe}$ function was calculated from the complete set of natural assemblages, using the Mg-Al-celadonite and $W^G_{Al–Mg}$ parameters obtained above. The different pressure–temperature domains (HP–LT and HT, and LP–LT and HT) placed constrains on the pressure and temperature dependencies of $W^G_{Al–Fe}$. To obtain the preliminary values $W^H_{Al–Fe}$, $W^S_{Al–Fe}$ and $W^V_{Al–Fe}$, we used a trial and error method to fit the pressures and temperatures recalculated in the step above with the Al-Mg-celadonite end member.

To avoid the influence of the K–Na, K–*v* and Na–*v* interactions on the equilibrium constant, we discarded equilibria involving paragonite and/or feldspar. Again, since muscovite and Al-Mg-celadonite are the only K-bearing phase components, they appear with the same stoichiometric coefficients in the equilibria involving phengite, and the K–Na, K–*v* and Na–*v* interactions cancel out in the equilibrium constant. Because no distinction is made between Fe^{2+} and Fe^{3+}, Fe^{3+}–Al and Fe^{2+}–Al interactions are assumed to be identical.

Entropy and enthalpy of Fe-Al-celadonite

The P_{ref}–T_{ref} conditions of the input data were then recalculated with the Al-Mg-celadonite standard-state properties and Margules parameters obtained above ($W^G_{Al–Mg}$ and $W^G_{Al–Fe}$): P_{KMASH} and T_{KMASH}. The standard-state thermodynamic properties of Fe^{2+}-Al-celadonite and the final $W^G_{Al–Fe(P,\ T)}$ function were estimated from the simultaneous consideration of the experiments of Massonne and Szpurka (1997) in the KFASH system, the Fe–Mg partitioning between phengite and garnet (Krogh and Raheim 1978; Green and Hellman 1982) or chlorite (most of the natural data listed in Table 5). As shown in Fig. 5b, V^0 of Al-Fe^{2+}-celadonite is not well constrained by the experiments of Massonne and Szpurka

(1997). It was thus optimized during the data extraction with an objective function aimed at keeping the volume as close as possible to the value obtained by the regression analysis on experimental results. Final values of H^0, S^0 and V^0 of Fe-Al-celadonite are reported in Table 6.

For each KWM–Gt or KWM–Chl natural assemblage, the conditions of equilibrium are given by Eqs. 1 and 2, with

$$K_{Chl-KWM} = a_{Daph}.a^{5}_{Al-Mg-cel}.a^{-1}_{Clin}.a^{-5}_{Al-Fe-cel} \quad (4)$$

or

$$K_{Gt-KWM} = a_{Alm}.a^{3}_{Al-Mg-cel}.a^{-1}_{Prp}.a^{-3}_{Al-Fe-cel} \quad (5)$$

and

$$K\Delta_r G^0 = \Delta_r H^0 - T.\Delta_r S^0 + \int_{T^0}^{T} C_p.dT - T.\int_{T^0}^{T} Cp/_T.dT + \int_{P^0}^{P} V.dP \quad (6)$$

For exchange reactions, the term $[\int_{T^0}^{T} C_p.dT - T.\int_{T^0}^{T} Cp/_T.dT]$ can be neglected and $\int_{P^0}^{P} V.dP = (P-1)\,\Delta_r V^0$ Equation (6) was therefore approximated as

$$\Delta rG^0 = A - B.T + (P-1).C \quad (7)$$

with $A = H^0_{Fe\text{-}Al\text{-}cel} + A1$, $B = S^0_{Fe\text{-}Al\text{-}cel} + B1$, and $C = V^0_{Fe\text{-}Al\text{-}cel} + C1$. A1, B1 and C1 are computed from the known standard-state properties of Al-Mg-celadonite, daphnite and clinochlore or almandine and pyrope.

Combining Eq. (7) with Eqs. (4) or (5), the standard-state thermodynamic data of Fe-Al-celadonite can be computed from the equilibrium constants for the KWM–Chl or KWM–Gt exchange reactions using the following equation:

$$H^0_{Fe-Al-cel} - T.S^0_{Fe-Al-cel} + P.V^0_{Fe-Al-cel} = A1 - T.B1 + P.C1 - RT.\ln K \quad (8)$$

with K calculated for each mineral pair for known P and T.

A multilinear least-square method was used to extract the H^0, S^0, and V^0 of Al-Fe^{2+}-celadonite from the experimental (Massonne and Szpurka 1997) and natural constraints simultaneously.

The pyrophyllitic and paragonitic substitutions

The $W^G_{(K-Na)A(P,\,T)}$, $W^G_{(Na-v)A(P,\,T)}$ and $W^G_{(K-v)A(P,\,T)}$ functions were calculated by a trial and error method, using natural constraints, experimental data in the

Table 7. Results obtained for the excess properties of the pyrophyllitic and paragonitic solid solutions, using the natural data set of Table 5 and available experiments (see text)

	(A) Na–K (J/mol)	(A) Na–*v* (J/mol)	(A) K–*v* (J/mol)
W^H 1–2	12,230	40,000	35,000
2–1	19,456	40,000	45,000
W^S 1–2	–5	5	25
2–1	–1.65	5	10
W^V 1–2	0.67	0.00	–0.85
2–1	–0.46	0.00	–0.85

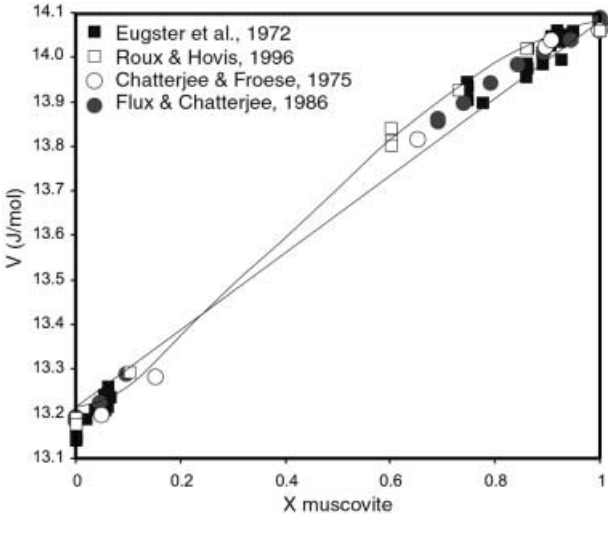

Fig. 6. V for the muscovite–paragonite binary. The least-square analysis leads to an asymmetrical solid solution with Margules parameters similar to the values estimated by Chatterjee and Froese (1975). The resulting values are reported in Table 7. We kept the V^0 of muscovite and paragonite unchanged from the data set of Berman (1988) to preserve the consistency

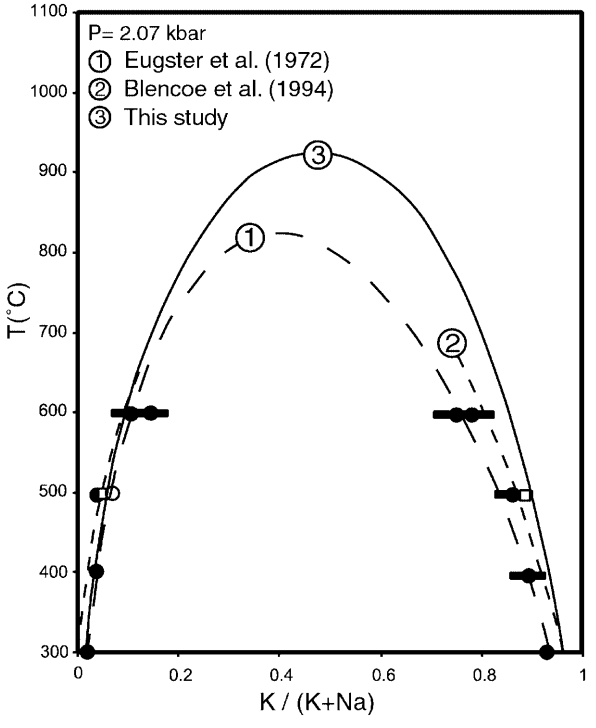

Fig. 7. Paragonite–muscovite solvus in the NKASH system at 2.07 kbar (*continuous line*). The *dashed lines 1* and *2* represent the solvus obtained by Chatterjee and Froese (1975) and Blencoe et al. (1994), respectively

Table 8. T estimates using TWQ software (Berman 1988) for the Na–K exchange between KWM and feldspar, at the P given by Green and Usdansky (1986; *G-U*). The results are in very good agreement with the temperatures previously estimated either by the garnet–biotite geothermometer (see references below) or the feldspar–muscovite geothermometer (Green and Usdansky 1986). *N.a.* Not applicable

Sample	T calculated with different geothermometers[a]						P (bar)	T (°C)
	F-S	P-G	H-S	H-L	G-S	G-U		
Penfold Creek (Fletcher and Greenwood 1978)								
5	596	560	668	617	599	674	7,000	596
6	534	596	553	549	523	565	7,000	486.5
7	648	676	663	626	577	561	7,000	498
8	572	628	600	576	545	488	7,000	413.5
9	521	577	538	536	510	505	7,000	441.5
11	539	599	573	553	525	558	7,000	490
12	602	630	617	596	568	508	7,000	447
13	625	677	640	613	585	585	7,000	543
14	631	700	659	617	619	625	7,000	564
15	640	674	650	621	623	466	7,000	425.5
Azure Lake (Pigage 1982)								
373	545	602	573	557	545	565	5,678	523
121	535	651	603	578	535	581	5,546	536.5
82	525	626	549	542	524	552	5,133	523
398	541	652	557	553	544	562	5,528	512.5
492	543	618	579	569	534	505	5,979	477
223	533	621	570	556	529	601	6,035	537
2-376	555	641	585	564	547	592	5,828	552
2-13	523	656	552	542	535	600	5,396	567
74	581	658	612	585	578	569	6,731	500.5
59	557	682	581	565	549	579	5,828	543
40	540	580	558	553	530	500	5,264	484.5
Mt. Moosilauke (Hodges and Spear 1982)								
78B	468	533	477	499	488	514	3,918	494
80D	489	565	512	518	513	588	3,444	581.5
92D	491	557	501	518	508	422	3,493	394.5
145E	498	567	507	524	524	441	3,167	418.5
146B	519	621	538	540	527	531	2,722	539.5
146D	464	561	480	498	486	532	2,677	534
Augusta, Maine (Ferry 1978, 1979)								
694s	n.a.	n.a.	n.a.	n.a.	n.a.	676	3,500	372.5
698s	n.a.	n.a.	n.a.	n.a.	n.a.	364	3,500	359
821s	n.a.	n.a.	n.a.	n.a.	n.a.	474	3,500	467.5
838s	n.a.	n.a.	n.a.	n.a.	n.a.	446	3,500	415
276s	n.a.	n.a.	n.a.	n.a.	n.a.	401	3,500	408.5
787s	n.a.	n.a.	n.a.	n.a.	n.a.	315	3,500	315

[a]Garnet–biotite thermometer calibrations: F-S, Ferry and Spear (1978); P-G, Pigage and Greenwood (1982); H-S, Hodges and Spear (1982); H-L, Holdaway and Lee (1977); G-S, Ganguly and Saxena (1984). Plagioclase–muscovite thermometer calibrations: G-U, Green and Usdansky (1986); s, secondary muscovite; T, plagioclase–muscovite geothermometer (this study). Feldspar crystalline solutions: solid solution parameters of Fuhrman and Lindsley (1988) and thermodynamic properties of Berman (1988)

KNASH system, and the natural observations on the solvus between KWM and pyrophyllite.

K–Na exchange at the A site

These parameters were optimized with an objective function aimed at keeping the values as close as possible to the values calculated by Chatterjee and Froese (1975). W^{V}_{K-Na} was calculated by a least-square method using the experimental estimates of the white micas volume as a function of Na content (Zen et al. 1964; Burnham and Radoslovich 1964; Guven 1971; Rothbauer 1971; Eugster et al. 1972; Chatterjee 1974; Chatterjee and Johannes 1974; Flux and Chatterjee 1986; Roux and Hovis 1996).

Our results (Fig. 6; Table 7) are similar to the values proposed by Chatterjee and Froese (1975). The W^{H}_{K-Na}, W^{H}_{Na-K}, W^{S}_{K-Na} and W^{S}_{Na-K} were extracted by considering simultaneously the Na–K exchanges between experimental KWM and paragonite (Fig. 7; Eugster et al. 1972), and between natural KWM and feldspar (Table 8; thermometer of Green and Usdansky 1986, estimated from natural data of Ferry 1978, 1979, Fletcher and Greenwood 1978, Hodges and Spear 1982, and Pigage 1982).

K–v exchange at the A^{XII} site

$W^{G}_{(K-v)A(P,\,T)}$ and $W^{G}_{(v-K)A(P,\,T)}$ functions were calculated using natural data (Table 5) together with the data of Frey et al. (1988; closed circles), Jiang et al. (1990; open circles), and Giorgetti et al. (1998; open squares) on the

KWM–pyrophyllite solvus (Fig. 8a). The results are presented in Table 7.

Na–v exchange at the A^{XII} site

The $W^{G}_{(Na-v)A(P,\ T)}$ and $W^{G}_{(v-Na)A(P,\ T)}$ are not well constrained since very few data exist on the paragonite–pyrophyllite solvus. The influence of pressure on this solvus is completely unknown. For this reason, we set the $W^{V}_{(Na-v)A}$ and $W^{V}_{(v-Na)A}$ to zero. We optimized the remaining parameters in order to fit the P–T references of the natural data set and to keep the solvus as open as possible. The results are presented on Fig. 8b.

Results and discussion

Thermodynamic properties of Mg-Al-celadonite and the W^{G}_{Al-Mg} and W^{G}_{Al-Fe} parameters

The results on the thermodynamic properties of Mg-Al-celadonite and the W^{G}_{Al-Mg} and W^{G}_{Al-Fe} parameters are listed in Table 6, together with the data of Massonne and Szpurka (1997) and Holland and Powell (1998). The entropy of Mg-Al-celadonite is slightly higher than the entropy proposed by Holland and Powell (1998) and Massonne and Szpurka (1997), but still within the standard deviation proposed by the authors (Massonne and Szpurka 1997). Using these thermodynamic properties, we have reported in Figs. 9 and 10 the calculated location of the KWM Si isopleths for the mineralogical assemblages investigated experimentally by Massonne and Szpurka (1997).

Our solid-solution model implies that the Mg(M2) content is influenced not only by the TK substitution but also by the DT substitution. As a consequence, for each Tschermak content isopleth (fixed Si content), the uncertainty due to errors on the trioctahedral KWM content is represented by shaded bands. It appears that the isopleths calculated for KWM compositions close to muscovite have a larger uncertainty than those closer to the Al-celadonite end member. The results of calculation are in agreement (within the experimental uncertainties) with all the constraints provided by the FkPQ and PyKQ/C equilibria, except for three and one brackets, respectively. Nevertheless, it must be noted that the calculated Si content of KWM in equilibrium with pyrope, kyanite and quartz/coesite is systematically above that determined experimentally. As we state above, this is due to the use of low-temperature natural data to derive the relevant thermodynamic properties.

Using the calculated Mg-Al-celadonite standard-state properties and the W^{G}_{Al-Mg} and W^{G}_{Al-Fe} parameters, it is also possible to re-estimate the equilibrium conditions for the natural samples used as input data. The results (P_{calc} and T_{calc}) are reported in Fig. 11 versus the reference pressures and temperatures (P_{ref} and T_{ref}, see Table 5). As explained above, P_{ref} and T_{ref} were either estimated (when more than two independent equilibria could be calculated without considering KWM), or they correspond to the original pressure and temperature ranges given by the authors when less than two equi-

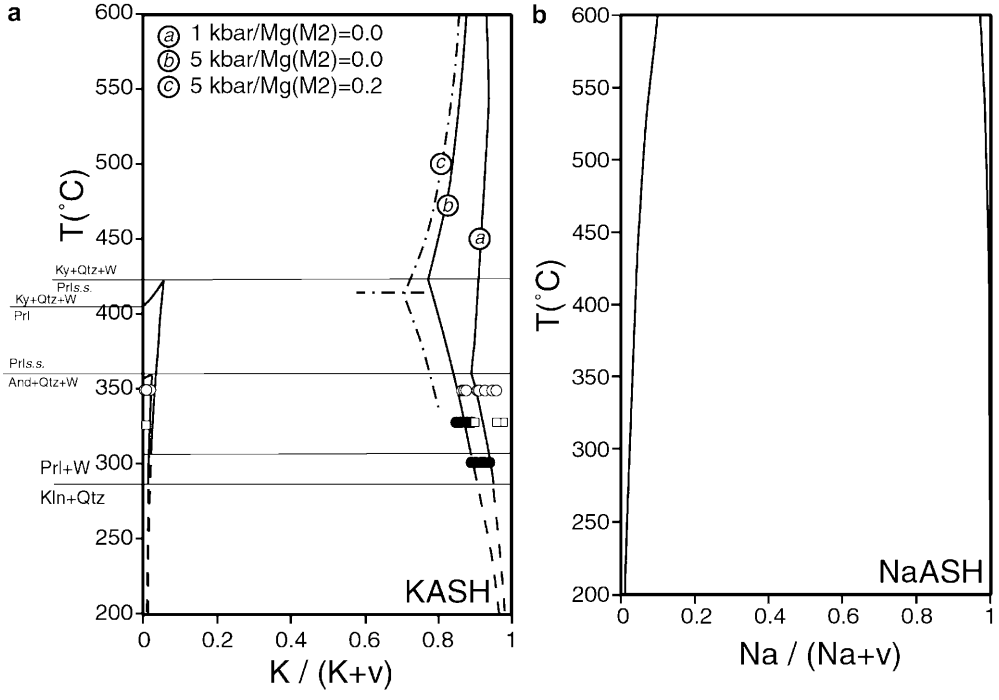

Fig. 8. **a** Pyrophyllite–muscovite solvus in the KASH system at 1 and 5 kbar (*a* and *b* solvi), and for two Tschermak exchanges at 5 kbar (Mg(M2) = 0.0 and 0.2; *c* solvus). The data are from Giorgetti et al. (1998; *closed circles*), Jiang et al. (1990; *open circles*), and Frey et al. (1988; *open squares*). **b** Paragonite–pyrophyllite solvus in the NaASH system. Due to the lack of paragonite–pyrophyllite occurrences and experimental data, the solvus is not very well constrained and should be considered with caution

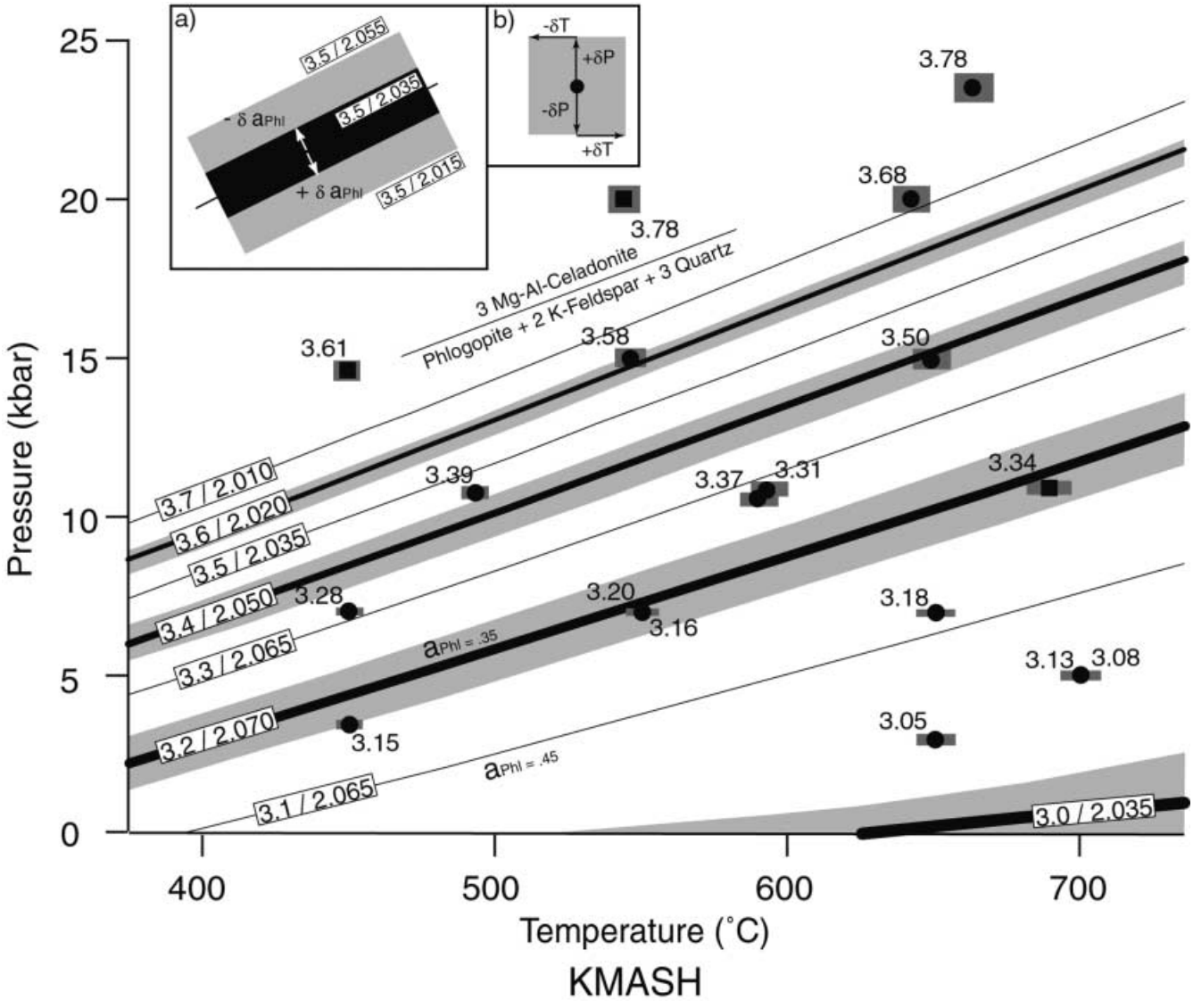

Fig. 9. Results on the recalculated KWM Tschermak isopleths in the presence of phlogopite–K-feldspar–quartz and water (KMASH system), using the thermodynamic data and Margules parameters reported in Table 6. *Numbers* refer to the Si content determined by XRD (Massonne and Schreyer 1986). *Closed circles* represent experimental data (Massonne and Szpurka 1997) fitted by the present solid-solution model, whereas *closed squares* represent outliers. Location of the isopleths is dependent on the activity of phlogopite (the 2σ uncertainty on this activity is symbolized by the thickness of the *continuous lines*), and on the KWM trioctahedral content (the 2σ uncertainty associated to the trioctahedral content of KWM is represented by the *shaded areas*). Experimental uncertainties on pressure and temperature are represented by the *shaded squares* around the *closed circles* and *squares*

libria could be calculated. Standard deviations of $\pm 2{,}000$ bar and ± 50 °C were introduced on P_{ref} and T_{ref}, respectively, to account for the precision of the P–T estimates, except when the authors give explicitly greater standard deviations.

The temperature and pressure conditions calculated with the new thermodynamic data for Mg-Al-celadonite (Table 6) are in agreement with the reference values (closed circles in Fig. 11), except for three sets of data (open circles, squares and diamonds).

1. The temperature and pressure conditions estimated for the LP–LT samples from Leoni et al. (1998) are higher than those estimated by Leoni et al. (1996, 1998; open circles). However, these high-pressure estimates are not surprising, since the composition of the KWM in these samples is similar to those of KWM occurring with carpholite in the HP–LT samples (cf. Bousquet et al. 1998; Agard 1999). Higher pressure conditions than reported by Leoni et al. (1998) are also suggested by the occurrence of blue amphibole in metabasites and carpholite in metapelites of the Cravasco-Voltaggio unit (B. Goffé and L. Martin, personal communication).
2. The pressure conditions calculated for the HP–LT data of Theye and Seidel (1991; open squares) are lower than the values previously estimated by these authors. The different KWM compositions (Si content from 3.4 to 3.2) reported by Theye and Seidel

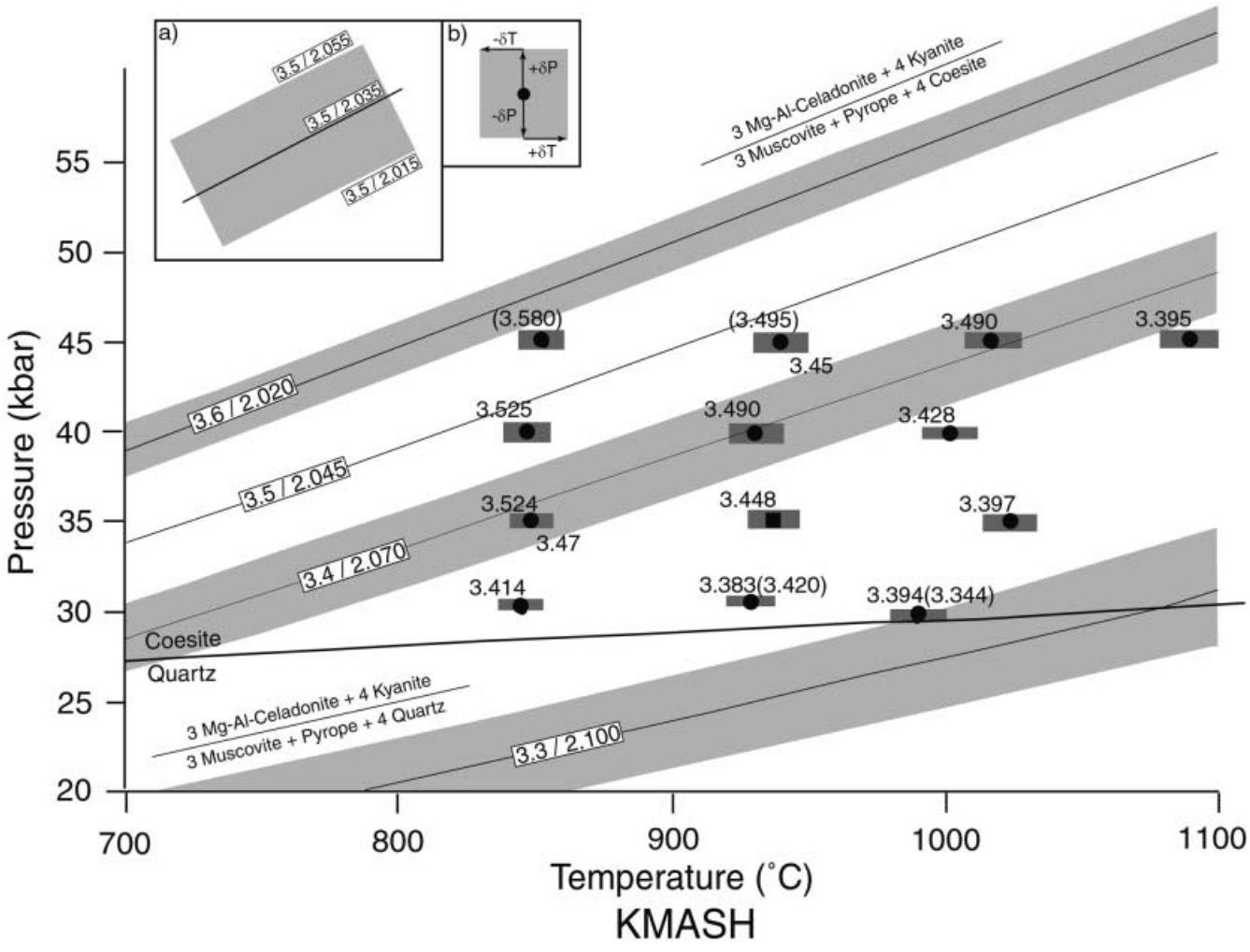

Fig. 10. Results on the recalculated KWM Tschermak isopleths in the presence of kyanite–pyrope–quartz or coesite and water (KMASH system), using the thermodynamic data and Margules parameters reported in Table 6. *Numbers* refer to the Si content determined either by XRD (Massonne and Schreyer 1986) or by EMPA (within *brackets*). *Closed circles* represent experimental data (Massonne and Szpurka 1997) fitted by the present solid-solution model, whereas *closed squares* represent outliers. Location of the isopleths is dependent on the KWM trioctahedral content (the 2σ uncertainty associated to the trioctahedral content of KWM is represented by the *shaded areas*). Experimental uncertainties on pressure and temperature are represented by the *shaded squares* around the *closed circles* and *squares*

(1991) yield pressures ranging between 15 and 9 kbar and correspond probably to different crystallization episodes during uplift. More important discrepancies are observed between the temperatures proposed by Theye and Seidel (1991) and our estimates (up to 150 °C). However, the equilibrium which constrains temperature (Fe–Mg exchange between chloritoid and chlorite) is independent of KWM.

3. Some of the HP–HT data of Sambagawa (open squares) yield temperatures and pressures largely below the peak of metamorphism calculated by Enami et al. (1994). In these samples, the KWM compositions differ from those related to the peak of metamorphism, and correspond to strong retrogression of the metapelites into the greenschist facies (Vidal and Parra 2000).

For the LP–HT data, the equilibria with the Al-Mg-celadonite end member are very sensitive to the Mg content of the M2 site. In particular, Figs. 9 and 10 show that recalculated isopleths are very sensitive to the trioctahedral and Al-celadonite contents when KWM are close to the muscovite end member, and that using the Mg-Al-celadonite end member leads to large uncertainties in the P–T estimates. Consequently, the Al-Mg-celadonite end member should not be taken into account for this type of paragenesis. When considering only the muscovite end member, there is a good agreement between the P–T conditions which we estimate and the pressure derived with the geobarometer of Hoisch (1990) at the same temperature.

Thermodynamic properties of Fe-Al-celadonite

The entropy of Fe-Al-celadonite derived in the present study is slightly higher than the value of Holland and Powell (1998), and the enthalpy is very different from the

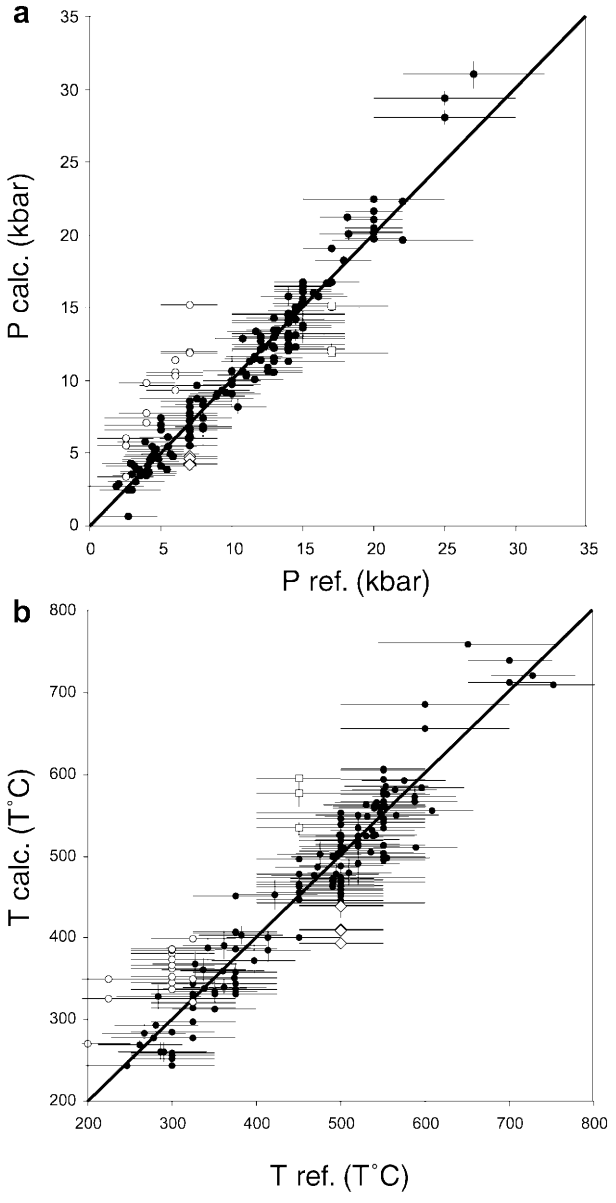

Fig. 11a, b. Comparison between **a** pressure and **b** temperature calculated with the new thermodynamic data (Table 6) and the pressure and temperature of reference for the optimization (P_{ref} and T_{ref}). P_{ref} and T_{ref} are either the results given by Intersx software (Berman 1991) or the P–T references given by the authors (Table 5, last column). *Closed symbols* correspond to $P–T_{calc} \approx P–T_{ref}$. Outliers are represented by *open circles* (Leoni et al. 1996, 1998), *open squares* (Theye and Seidel 1991), and *open diamonds* (some data of the Sambagawa Belt, this study). These discrepancies are discussed in the text

values proposed by these authors and Massonne and Szpurka (1997). However, the Si isopleths calculated with the new thermodynamic data are consistent with all the experimental results reported by Massonne and Szpurka (1997), except one (Fig. 12).

In Fig. 13a, b, we have plotted $deltaP = (P_{KFASH} – P_{KMASH})$ and $deltaT = (T_{KFASH} – T_{KMASH})$ for all the natural data (Table 5). P_{KFASH} and T_{KFASH} were calculated using the Al-Fe-celadonite end member with the Intersx software after having eliminated the most composition-dependant equilibria (Berman 1991; Lieberman and Petrakakis 1991). P_{KMASH} and T_{KMASH} correspond to the P–T results calculated with the Mg-Al-celadonite end member, but without considering the Fe-Al-celadonite end member. Standard deviations of $\pm 1{,}000$ bar and ± 50 °C were introduced on P_{KMASH} and T_{KMASH} to account in particular for the assumption that all iron in KWM is divalent. In most cases, the P–T estimates obtained with Al-Fe^{2+}-celadonite agree well with those obtained without this end member. However, some data do not lie on the zero line (within errors). The calculated temperatures are always constrained by the Fe–Mg exchange between KWM and another Fe-Mg-bearing mineral (garnet or chlorite), with Fe-celadonite on the high-temperature side of the exchange reaction. The ncorporation of Fe^{3+} decreases the activity of Fe-Al-celadonite, and shifts the location of such Fe–Mg equilibria at low temperature. Therefore, T_{KFASH} higher than T_{KMASH} ($deltaT > 0$) can be easily explained by the presence of Fe^{3+} in KWM. Data for which $T_{KFASH} < T_{KMASH}$ ($deltaT < 0$) are more difficult to explain, but they always correspond to P_{KMASH} and T_{KMASH} estimated by only two independent equilibria (i.e., the system of chemical equations is not overdetermined), so that equilibrium cannot be demonstrated. A tentative explanation is that these KWM correspond to late phases crystallizing during decompression and which are not equilibrated with the other minerals formed at higher P and T.

For each pressure domain, we have plotted in Fig. 14a the equilibrium constant $lnK_{Chl–KWM}$ (see Eq. 4) of natural chlorite–KWM pairs as a function of the reverse of the temperature estimated above with the new thermodynamic data for Mg-Al-celadonite. These data are compared with the lnK predicted when using the standard-state properties of Mg- and Fe-Al-celadonite and the mixing properties derived in the present study (Table 6). It appears that pressure and temperature dependency evidenced from the lnK predicted when using both Mg- and Fe-celadonite end members is in good agreement with that observed from original lnK values. In Fig. 14b, we have plotted the predicted vs. observed lnK of chlorite–KWM pairs. The strong correlation between the calculated and observed lnK lends credibility to the thermodynamic data derived for KWM and demonstrates their agreement with the chlorite solid-solution model derived by Vidal et al. (2001).

The geothermometer of Krogh and Raheim (1978; continuous lines) at three different pressures, 10, 30 and 35 kbar, and the three geothermometers of Green and Hellman (1982; dashed lines) at two different pressures, 10 and 30 kbar, are shown as a function of 1/T in Fig. 15. Using the standard-state properties derived in this study, we have recalculated the equilibrium temperature for each experiment (squares: Green and Hellman 1982; circles: Krogh and Raheim 1978). We have also reported the calculated equilibrium temperature for three garnet–KWM natural pairs stable at about 10 kbar (Arenas et al. 1995; diamonds). It appears that our data are in good

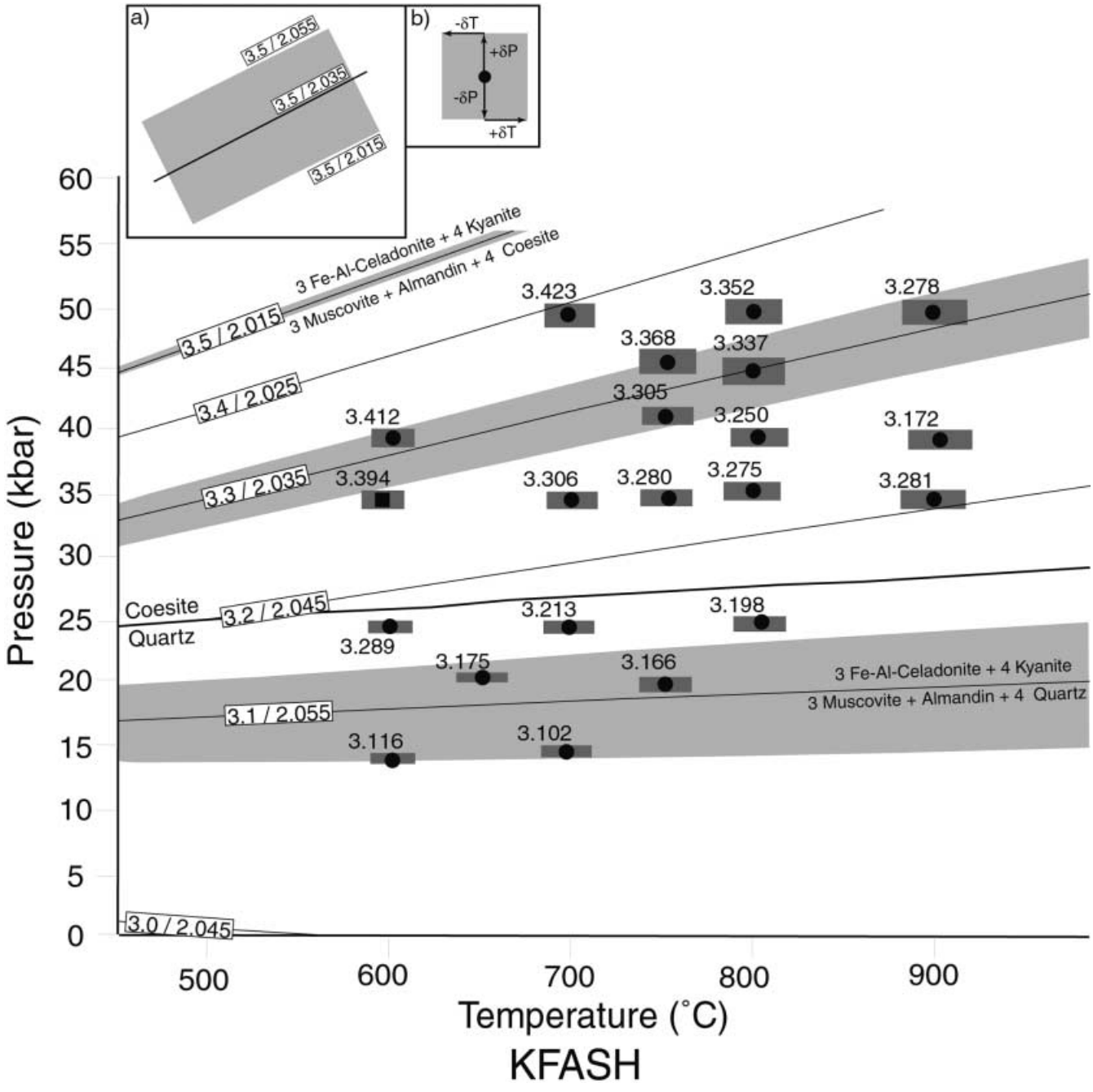

Fig. 12. Results on the recalculated KWM Tschermak isopleths in the presence of kyanite–almandine–quartz or coesite and water (KFASH system), using the thermodynamic data and Margules parameters reported in Table 6. *Numbers* refer to the Si content determined by XRD (Massonne and Schreyer 1986). *Closed circles* represent experimental data (Massonne and Szpurka 1997) fitted by the present solid-solution model, whereas *closed squares* represent outliers. Location of the isopleths is dependant on the KWM trioctahedral content (the 2σ uncertainty associated to the trioctahedral content of KWM is symbolized by the *shaded areas*). Experimental uncertainties on pressure and temperature are represented by the *shaded squares* around the *closed circles* and *squares*

agreement with the high-pressure experiments of Krogh and Raheim (1978), but in better agreement with the geothermometers of Green and Hellman (1982) for the medium-pressure natural samples of Arenas et al. (1995).

The $W^{G}_{Na–K}$ and $W^{G}_{K–Na}$ parameters

The results are presented in Table 7. The parameters W^{H}, W^{V} and W^{S} are similar to those estimated by Chatterjee and Froese (1975), except $W^{S}_{K–Na}$ which reached –5 after optimization, against –0.71 for these authors. This is due to the consideration of natural KWM–feldspar or KWM–paragonite pairs, for which temperatures calculated with the solid-solution model of Chatterjee and Froese (1975) are systematically too low

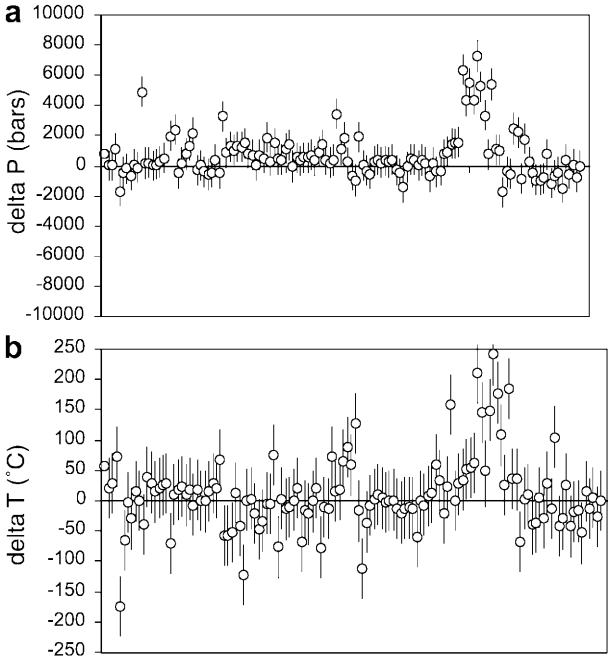

Fig. 13. **a** DeltaP = P_{KFASH}–P_{KMASH} and **b** deltaT = T_{KFASH}–T_{KMASH} for all carboneous-bearing samples of Table 5. P_{KMASH} and T_{KMASH} are the results given by Intersx software (Berman 1991) using the Al-Mg-celadonite end member and based on an independent set of equilibria. P_{KFASH} and T_{KFASH} are the P–T estimates of Intersx software, using the thermodynamic data of Al-Fe-celadonite end member and solid-solution properties in Table 6 (see text for further explanations)

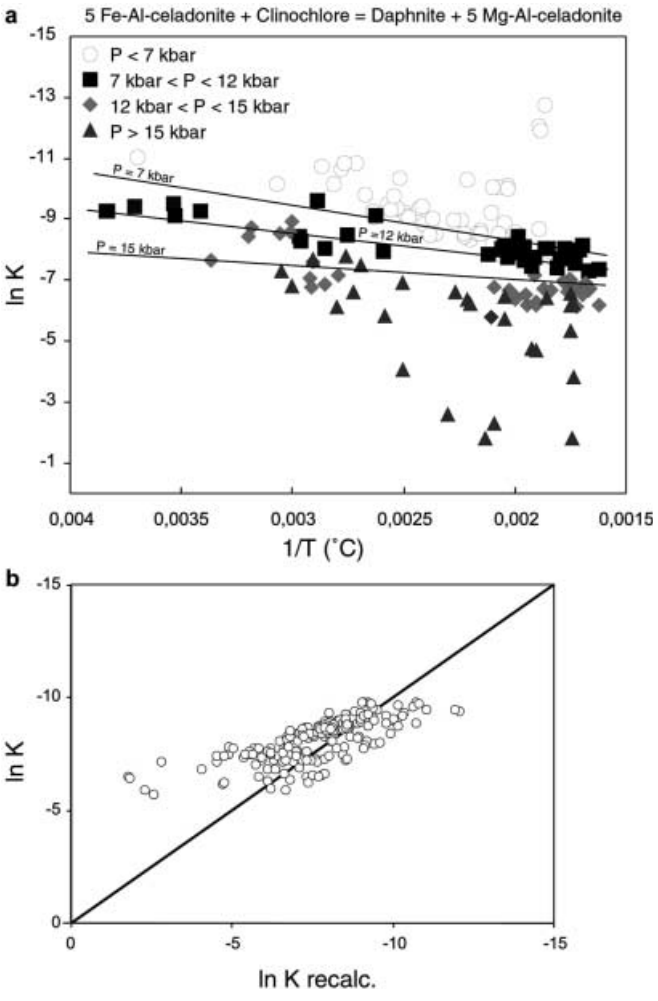

Fig. 14. **a** lnK versus 1/T (°C) for the equilibrium 5Fe-Al-celadonite + clinochlore = daphnite + 5Mg-Al-celadonite, showing that lnK is extremely dependent not only on temperature but also on pressure. *Lines* represent the results of the multilinear analysis delimitating the different pressure domains. **b** Observed lnK versus recalculated lnK using the thermodynamic data and excess properties of Table 6 (see text for the optimization procedure). The fit is very good for lnK between –5 and –11 where the *circles* lie on the continuous *line*

with respect to the results of Green and Usdansky (1986) and our independent estimates. In order to resolve this problem, the Na–K solvus needs to be more open and W^S was adjusted. The results for the KWM–feldspar equilibrium using the solid-solution model of Table 7 are presented in Table 8. The temperature estimates are in very good agreement with the geothermometer of Green and Usdansky (1986).

The $W^G_{v–A}$ and $W^G_{A–v}$ parameters

Results for the $W^G_{v–K}$, $W^G_{K–v}$ and the $W^G_{Na–v}$, $W^G_{v–Na}$ parameters are also presented in Table 7. In Figs. 8a and 16, we plotted the muscovite–pyrophyllite solvi for two different pressures (Fig. 8a: 1 and 5 kbar; Fig. 16: 5 and 10 kbar) and two Mg-Al-celadonite contents (Mg (M2) = 0.0 and 0.2 a.p.f.u. at 5 kbar).

In Fig. 8a, we also reported the $K/(K+v)$ of coexisting KWM and pyrophyllite (open squares: Giorgetti et al. 1998; closed circles: Frey et al. 1988; open circles: Jiang et al. 1990). In Fig. 16, we added the $K/(K+v)$ ratio of natural KWM for two ranges of pressures (closed and open squares: $P < 5$ kbar and $5 < P < 10$ kbar, respectively). These two figures indicate the good agreement between the natural observations and the calculated solvi for different pressures and Tschermak contents. In particular, at a given pressure the temperature tends to increase the pyrophyllitic content of KWM until the pyrophyllite–kyanite reaction. From this temperature, the pyrophyllitic content decreases. At a given temperature, the pressure and the Tschermak content tend to increase the pyrophyllitic content of KWM.

$W^G_{Na–v}$ and $W^G_{v–Na}$ parameters were also calculated from the natural data. However, because of the lack of constraints, these parameters are only provisional values and should be considered with caution.

Concluding remarks

The phengite solid solution and the Al-celadonite standard-state properties calculated in the present study are

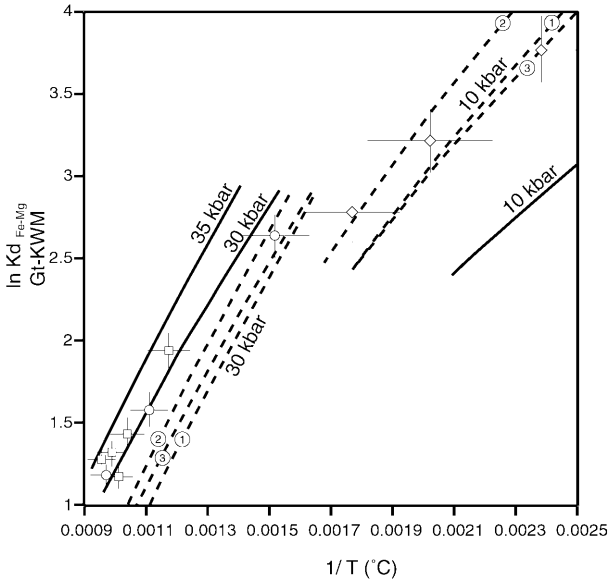

Fig. 15. $\ln K_D$ Fe/Mg of KWM–garnet versus 1/T (°C). *Continuous lines* represent the geothermometer of Krogh and Raheim (1978) at 35, 30 and 10 kbar. *Dashed lines* represent the geothermometers of Green and Hellman (1982) for the different bulk-rock compositions: *1* Ca systems with Mg/(Fe + Mg) close to 0.67; *2* low-Ca systems with Mg/(Fe + Mg) between 0.20 and 0.30; *3* basaltic systems with Mg/(Fe + Mg) close to 0.67. *Squares* and *circles* represent the experiments of Green and Hellman (1982), and Krogh and Raheim (1978), respectively, for which temperatures are calculated with thermodynamic data and excess properties of Table 6, at the pressure given by the authors. *Diamonds* represent garnet–KWM occurrences of Arenas et al. (1995) whose P–T conditions of crystallization have been estimated to 10 kbar at around 500 °C. Our new solid-solution model best fits the Krogh and Raheim (1978) geothermometer at high pressure, and the Green and Hellman (1982) geothermometers at lower pressure

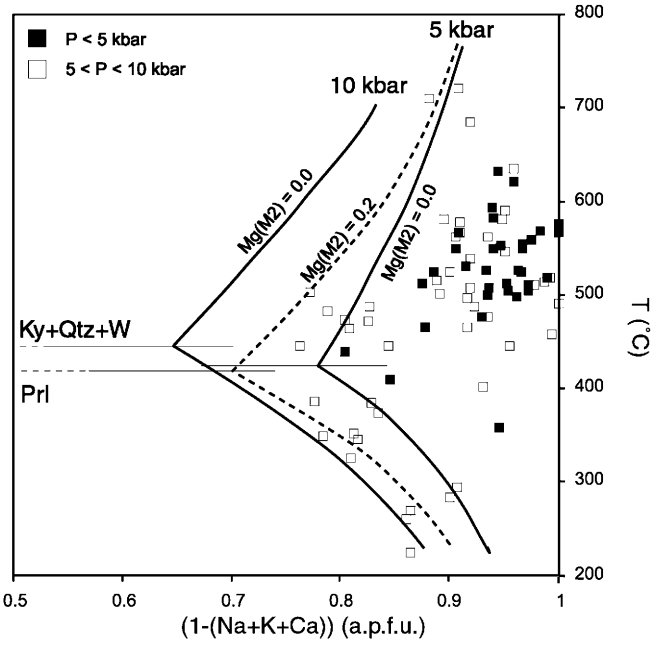

Fig. 16. Muscovite–pyrophyllite solvi calculated for two different pressures (5 and 10 kbar) at Mg(M2) = 0.0, and for Mg(M2) = 0.2 at 5 kbar. *Closed* and *open squares* represent the unlimiting assemblages which crystallized at pressures under 5 and 10 kbar, respectively

consistent with the data set of Berman (1988), the standard-state properties for Mg- and Fe-chloritoid (Vidal et al. 1994, 1999) as well as Mg-carpholite (Vidal et al. 1992), and the new standard-state properties and solid-solution parameters for garnet (Berman 1990) and chlorite (Vidal et al. 2001).

There are several conditions for the entire data set to be applied. Firstly, the chemical analysis must be described by the decomposition on the seven end members (muscovite, Al-Mg-celadonite, Al-Fe-celadonite, phlogopite, annite, paragonite and pyrophyllite; see Appendix).

The second limitation is the real content of each end member in a given analysis. For KWM with a very low end-member content, it is not possible to use this end member to estimate the P–T conditions, mainly because a slight variation in its content will have a large impact on the P–T location of the equilibrium curves involving this end member. For high-temperature phengite, for example, the pyrophyllite content is in fact lower than the uncertainty which we have on the estimation of the vacancies at the A site.

The use of an increased number of KWM end members makes the estimation of pressure and temperature conditions possible even for high-variance parageneses, which was not possible by considering only muscovite, and sometimes Al-celadonite. It is therefore expected that a more continuous spatial assessment of the metamorphic P–T conditions at the outcrop scale will be possible (e.g., Vidal and Parra 2000). Another potential use of the phengite data calibrated in this study is the calculation of P–T paths using different generations and/or zoning of phengite coexisting in specific microstructures of the same thin section. In particular, the combination of phengite solid solution and chlorite solid solution allows one to evaluate local equilibrium at the thin-section scale, and provides constraints on the shape of the exhumation P–T paths of HP–LT rocks (Vidal and Parra 2000; Parra et al. 2002). Such constraints are generally difficult to obtain, since the rock mineralogy does not change significantly under greenschist facies conditions.

Acknowledgements Thanks are due to J. Ganguly for his constructive and helpful reviews and remarks, and to F. Trotet and L. Jolivet for their suggestions which improved an earlier version of the manuscript. This work was financially supported by the INSU program IT.

Appendix

Selection of the analyses

In order to discard contaminated analyses, we only retained EMP analyses with an oxygen sum between 92

and 96 wt% and showing less than 0.5 wt% ($TiO_2 + MnO + CaO$). Structural formulae were calculated on an 11-oxygen basis, assuming all iron to be divalent. Molar fractions of the seven end members (Mg- and Fe-Al-celadonite, muscovite, annite, phlogopite, paragonite, and pyrophyllite) in the remaining phengite compositions were calculated with six independent equations (one for each end member – the constraint $\Sigma X_{\text{end member}} = 1$). Finally, we only retained analyses which are strictly a linear combination of these end members and satisfy the following equalities.

Chemical constraints

- $(Mg + Fe)$ a.p.f.u.$-(X_{ACel} + 3X_{Phl} + 3X_{Ann}) = 0 \pm 0.075$
- K a.p.f.u.$-(X_{Ms} + X_{ACel} + X_{Phl} + X_{Ann}) = 0 \pm 0.075$
- Si a.p.f.u.$-(3X_{Ms} + 3X_{Pg} + 3X_{Phl} + 3X_{Ann} + 4X_{Prl} + 4\text{-}X_{ACel}) = 0 \pm 0.075$
- Al^{VI} a.p.f.u.$-(2X_{Ms} + 2X_{Pg} + 2X_{Prl} + X_{ACel}) = 0 \pm 0.075$

These criteria guarantee that KWM analyses are not contaminated by other minerals (e.g., quartz).

Exchange-vectors constrains

- $(Na + K)$ a.p.f.u.$-4 + (4X_{Prl} + 3(X_{Ms} + X_{Pg}))/(X_{Prl} + X_{Pg} + X_{Ms}) = 0 \pm 0.05$
- $((Mg + Fe)_{(M2)} - 2(Mg + Fe)_{(M1)} - 3 - (3X_{Ms} + 4X_{ACel})/(X_{Ms} + X_{ACel}) = 0 \pm 0.075$

where ± 0.075 and ± 0.05 stem from EMPA uncertainties.

The two latter criteria also ensure that the KWM analyses result from the exchange vectors chosen to model the solid solution for KWM. In particular, the effect of alkali volatilization leads to values significantly above zero, within microprobe errors for phengitic-rich KWM (Table 1, analyses 2 and 3) and can be thus easily detected. For phengitic-poor KWM, the alkali volatilization tends to decrease the ACel part which rapidly becomes negative, and can be also easily detected (Table 1, analysis 1).

From the initial set of 300 analyses, 250 fulfilled the above criteria. The deviation from the ideal, linear combination of the KWM compositions (Mg-ACel + Fe-ACel + Ms + Pg + Prl + Ann + Phl) is illustrated in Figs. 1 and 4. In Fig. 4, the recalculated Si content resulting only from the Tschermak exchange $((3X_{Ms} + 4X_{ACel})/(X_{Ms} + X_{ACel}))$ is plotted as a function of the $(Fe^{2+} + Mg)$ content corrected for the amount of biotite component $(= 2\bullet(Mg + Fe)_{(M1)})$. Ideally, all the analyses should plot on the 1:1 line between muscovite and Al-celadonite (TK substitution). The scatter resulting from errors due to EMPA analysis can be estimated with a Monte-Carlo method (Lieberman and Petrakakis 1991; Vidal and Parra 2000). Assuming a standard error of 1% for Si, Al, Mg, Mn, Fe and Ti oxides (Kohn and Spear 1991a, 1991b; Worley and Powell 2000), and 2% for K and Na oxides, the corresponding error on Si and $(Fe^{2+} + Mg)$ contents are 0.015 and 0.01 a.p.f.u., respectively. This is represented by the limiting dashed lines on Figs. 1 and 4. About 95% of the initial set of data plot in the "permissible domain", i.e., within the two dashed lines. It is noteworthy that the 5% remaining analyses also plot outside the "permissible domain" in Fig. 1, which shows the recalculated Si content resulting from only the pyrophyllitic exchange versus $(Na + K)$ content (uncertainty resulting from errors due to the EMPA: ± 0.025 a.p.f.u. for Si and $Na + K$). These analyses do not fit the criteria mentioned above and were simply discarded.

References

Agard P (1999) Evolution métamorphique et structurale des métapélites océaniques dans l'orogenèse Alpin: l'exemple des Schistes Lustrés des Alpes occidentales (Alpes Cottiennes). PhD Thesis, Université Paris VI

Agard P, Vidal O, Goffé B (2001) Interlayer and Si content of phengites in high-pressure carpholite-bearing metapelites. J Metamorph Geol 19:479–496

Aja SU (1995) Thermodynamic properties of some 2:1 layer clay minerals from solution-equilibration data. Eur J Mineral 7:325–333

Aja SU, Rosenberg PE (1992) The thermodynamic status of compositionally-variable clay minerals: a discussion. Clays Clay Miner 40:292–299

Aja SU, Rosenberg PE, Kittrick JA (1991a) Illite equilibria in solutions. I. Phase relationships in the system K_2O-Al_2O_3-SiO_2-H_2O. Geochim Cosmochim Acta 55:1253–1264

Aja SU, Rosenberg PE, Kittrick JA (1991b) Illite equilibria in solutions. II. Phase relationships in the system K_2O-Al_2O_3-MgO-SiO_2-H_2O. Geochim Cosmochim Acta 55:1365–1374

Arenas R, Rubio Pascual FJ, Diaz Garcia F, Martinez Catalan JR (1995) High-pressure micro-inclusions and development of an inverted metamorphic gradient in the Santiago Schists (Ordenes Complex, NW Iberian Massif, Spain): evidence of subduction and syncollisional decompression. J Metamorph Geol 13:141–164

Bailey SW (1975) Cation ordering and pseudosymmetry in layer silicates. Am Mineral 60:175–187

Bailey SW (1984a) Classification and structures of the micas. In: Bailey SW (ed) Micas. Mineralogical Society of America, Blacksburg, Rev Mineral 13

Bailey SW (1984b) Review of cation ordering in micas. Clays Clay Miner 32:81–92

Baldelli C, Franceschelli M, Leoni L, Memmi I (1989) Ferrimuscovite and celadonite substitutions in muscovite from Fe^{3+}-rich low grade psammitic rocks (Northern Apennines, Italy). Lithos 23:201–208

Banno S, Nakajima T (1992) Metamorphic belts of Japanese islands. Annu Rev Earth Planet Sci 20:159–179

Berman RG (1988) Internally-consistent thermodynamic data for minerals in the system Na_2O-K_2O-CaO-MgO-FeO-Fe_2O_3-$A1_2O_3$-SiO_2-TiO_2-H_2O-CO_2. J Petrol 29:445–522

Berman RG (1990) Mixing properties of Ca-Mg-Fe-Mn garnets. Am Mineral 75:328–344

Berman RG (1991) Thermobarometry using multi-equilibrium calculations: a new technique, with petrological applications. Can Mineral 29:833–855

Berman RG, Brown TH (1984) A thermodynamic model for multicomponent melts, with application to the system CaO-Al_2O_3-SiO_2. Geochim Cosmochim Acta 48:661–678

Berman RG, Brown TH (1985) The heat capacity of minerals in the system K_2O-Na_2O-CaO-MgO-FeO-Fe_2O_3-Al_2O_3-SiO_2-TiO_2-H_2O-CO_2: representation, estimation, and high temperature extrapolation. Contrib Mineral Petrol 89:168–183

Biino GG, de Capitani C (1995) Equilibrium assemblage calculations: a new approach to metamorphic petrology. Boll Mus Reg Sci Nat Torino 13(2):11–53

Blencoe JG (1974) Experimental study of muscovite-paragonite stability relations. PhD Thesis, Stanford University

Blencoe JG (1977) Molar volumes of synthetic paragonite-muscovite micas. Am Mineral 62:1200–1215

Blencoe JG, Guidotti CV, Sassi FP (1994) The paragonite-muscovite solvus. II. Numerical geothermometers for natural, quasibinary paragonite-muscovite pairs. Geochim Cosmochim Acta 58(10):2277–2288

Bousquet R (1998) L'exhumation des roches métamorphiques de haute pression-basse température: de l'étude de terrain à la modélisation numérique. Exemple de la fenêtre de l'Engadine et du domaine Valaisan dans les Alpes Centrales. PhD Thesis, Université Paris XI

Bousquet R, Oberhansli R, Goffé B, Jolivet L, Vidal O (1998) High pressure-low temperature metamorphism and deformation in the Bundnerschiefer of the Engadine window: implications for the regional evolution of the Eastern Central Alps. J Metamorph Geol 16:657–674

Bröcker M (1990) Die metamorphe vulkanosedimentäre Abfolge der Insel Tinos (Kykladen, Griechenland) – Geologie, Petrographie und Minerachemie einer gründschieferfaziell überprägten Hochdruck-/Niedrig temperatur-Abfolge. Geotekt Forsch 74:1–107

Burhnam CW, Radoslovich EW (1964) Crystal structures of coexisting muscovite and paragonite. Carnegie Inst Wash Year Book 63:232–236

Cathelineau M (1988) Cation site occupancy in chlorites and illites as a function of temperature. Clay Miner 23:471–485

Cathelineau M, Izquierdo G (1988) Temperature-composition relationships of authigenic micaceous minerals in the Los Azufres geothermal system. Contrib Mineral Petrol 100:418–428

Chatterjee ND (1974) X-ray powder pattern and molar volume of synthetic 2M-paragonite: a refinement. Contrib Mineral Petrol 34:288–303

Chatterjee ND, Flux S (1986) Thermodynamic mixing properties of muscovite-paragonite crystalline solutions at high temperatures and pressures and their geological application. J Petrol 27:677–693

Chatterjee ND, Froese E (1975) A thermodynamic study of the pseudobinary join muscovite-paragonite in the system $KAlSi_8O_8$-$NaAlSi_3O_8$-Al_2O_3-SiO_2-H_2O. Am Mineral 60:985–993

Chatterjee ND, Johannes W (1974) Thermal stability and standard thermodynamic properties of synthetic $2M_1$-muscovite $KAl(AlSi_3O_{10}(OH)_2)$. Contrib Mineral Petrol 48:89–114

Cheng W, Ganguly J (1994) Some aspects of multicomponents excess free energy models with subregular binaries. Geochim Cosmochim Acta 58:3763–3767

Chopin C (1985) Les relations de phases dans les métapélites de haute pression. Thèse Habilitation, Université de Pierre et Marie Curie, Paris VI

Chopin C, Monié P (1984) A unique magnesiochloritoid-bearing, high-pressure assemblage from the Monte Rosa, western Alps: petrologic and ^{40}Ar-^{39}Ar radiometric study. Contrib Mineral Petrol 87:388–398

DallaTorre M, Livi KJT, Veblen DR, Frey M (1996) White K-mica evolution from phengite to muscovite in shales and shale matrix melange, Diablo Range, California. Contrib Mineral Petrol 123:390–405

Dempster TJ (1992) Zoning and recrystallization of phengitic micas; implications for metamorphic equilibrations. Contrib Mineral Petrol 190(4):526–537

Droop GTR (1985) Alpine metamorphism in the south-east Tauern Window, Austria. 1. P-T variations in space and time. J Metamorph Geol 3:371–402

Enami M, Wallis SR, Banno S (1994) Paragenesis of sodic pyroxene-bearing quartz schists: implications for the P-T history of the Sambagawa belt. Contrib Mineral Petrol 116:182–198

Essene EJ, Peacor DR (1995) Clay mineral thermometry – a critical perspective. Clays Clay Miner 43(5):540–553

Eugster HP, Yoder HS (1955) Micas. Annu Rep Geophys Lab 54:124–129

Eugster HP, Albee AL, Bence AE, Thompson JBJ, Waldbaum DR (1972) The two-phase region and excess mixing properties of paragonite-muscovite crystalline solutions. J Petrol 13:147–179

Faryad SW (1995) Phase petrology and P-T conditions of mafic blueschists from the Meliata unit, West Carpathians, Slovakia. J Metamorph Geol 13:701–714

Feininger T (1980) Eclogite and related high-pressure regional metamorphic rocks from the Andes of Ecuador. J Petrol 21(1):107–140

Ferry JM (1978) Fluid interactions between granite and sediment during metamorphism, South central Maine. Am J Sci 278(8):1025–1026

Ferry JM (1979) A map of chemical potential differences within an outcrop. Am Mineral 64(9-10):966–985

Ferry JM (1992) Regional metamorphism of the Waits River formation, Eastern Vermont: delineation of a new type of giant metamorphism hydrothermal system. J Petrol 33(1):45–94

Ferry JM, Spear FS (1978) Experimental calibration of the partitioning of Fe and Mg between biotite and garnet. Contrib Mineral Petrol 66:113–117

Fletcher CJN, Greenwood HJ (1978) Metamorphism and structure of Penfold Creek Area, near Quesnel Lake, British Columbia. J Petrol 20:743–794

Flux S, Chatterjee ND (1986) Experimental reversal of the Na-K exchange reaction between muscovite-paragonite crystalline solutions and a 2 molal aqueous (Na, K)Cl fluid. J Petrol 27(3):665–676

Frey M, Robinson D (1999) In: Frey M, Robinson D (ed) Low grade metamorphism. Blackwell, London

Frey M, Hunziker JC, Jaeger E, Stern WB (1983) Regional distribution of white K-mica polymorphs and their phengite content in the central Alps. Contrib Mineral Petrol 83(1-2):185–197

Frey M, Saunders J, Schwander H (1988) The mineralogy and metamorphic geology of low grade metasediments, Northern Range, Trinidad. J Geol Soc Lond 145:563–575

Furhman ML, Lindsey DH (1988) Ternary-feldspar modeling and thermometry. Am Mineral 73:201–215

Ganguely J, Saxena SK (1984) Mixing properties of alumino-silicate garnets: constraints from natural and experimental data, and application to geothermobarometry. Am Mineral 69:88–97

Giaramita MJ, Day HW (1991) Buffering in the assemblage staurolite-aluminium silicate-biotite-garnet-chlorite. J Metamorph Geol 9:363–378

Giorgetti G, Goffé B, Memmi I, Nieto F (1998) Metamorphic evolution of Verrucano metasediments in northern Apennines: new petrological constraints. Eur J Mineral 10:1295–1308

Gordon TM, Ghent ED, Stout MZ (1991) Algebraic analysis of the biotite-sillimanite isograd in the File Lake area, Manitoba. Can Mineral 29:673–686

Green TH, Hellman PL (1982) Fe-Mg partitioning between coexisting garnet and phengite at high pressure, and comments on a garnet-phengite geothermometer. Lithos 15:253–266

Green NL, Usdansky SI (1986) Toward a practical plagioclase-muscovite thermometer. Am Mineral 71:1109–1117

Guidotti CV, Sassi FP (1998a) Miscellaneous isomorphous substitutions in Na-K micas: a review, with special emphasis to metamorphic micas. Rend Fis Acc Lincei 9(9):57–78

Guidotti CV, Sassi FP (1998b) Petrogenetic significance of Na-K white mica mineralogy. Recent advances for metamorphic rocks. Eur J Mineral 10:815–854

Guidotti CV, Yates MG (1994) Petrogenetic implications of the Fe^{3+} content of muscovite in pelitic schists. Am Mineral 79:793–795

Guidotti CV, Sassi FP, Blencoe JG, Selverstone J (1994a) The paragonite-muscovite solvus. I. P-T-X limits derived from the

Na-K compositions of natural, quasibinary paragonite-muscovite pairs. Geochim Cosmochim Acta 58(10):2269–2275
Guidotti CV, Sassi FP, Sassi R, Blencoe JG (1994b) The effects of ferromagnesian components on the paragonite-muscovite solvus: a semi quantitative analysis based on chemical data for natural paragonite-muscovite pairs. J Metamorph Geol 12:779–788
Guven N (1971) The crystal structure of 2M1 phengite and 2M1 muscovite. Z Kristallogr 134:196–212
Haselton HT Jr, Cygan GL, Jenkins DM (1995) Experimental study of muscovite stability in pure H_2O and 1 molal KCl-HCl solutions. Geochim Cosmochim Acta 59(3):429–442
Heinrich CA (1982) Kyanite-eclogite to amphibolite facies evolution of hydrous mafic and pelitic rocks, Adula Nappe, Central Alps. Contrib Mineral Petrol 81:30–38
Heinrich CA (1986) Eclogite facies regional metamorphism of hydrous mafic rocks in the Central Alpine Adula Nappe. J Petrol 27(1):123–154
Hirajima T, Campagnoni R (1993) Petrology of a jadeite-quartz/coesite-almandine-phengite fels with retrograde ferro-nyboïte from Dora-Maira Massif, Western Alps. Eur J Mineral 5:943–955
Hodges KV, Spear FS (1982) Geothermometry, geobarometry and the Al_2SiO_5 triple point at Mt. Moosilauke, New Hampshire. Am Mineral 67:1118–1134
Hoisch TD (1990) Empirical calibration of six geobarometers for the mineral assemblage quartz + muscovite + biotite + plagioclase + garnet. Contrib Mineral Petrol 104:225–234
Holdaway MJ, Lee SM (1977) Fe-Mg cordierite stability in high grade pelitic rocks based on experimental, theoritical, and natural observations. Contrib Mineral Petrol 63(2):175–198
Holland TJB (1989) Dependence of entropy on volume for silicates and oxide minerals, a review and a predictive model. Am Mineral 74:5–13
Holland TJB, Powell R (1998) An internally consistent thermodynamic data set for phases of petrological interest. J Metamorph Geol 16:309–343
Hynes A, Forest RC (1988) Emperical garnet-muscovite geothermometry in low-grade metapelites, Selwyn Range (Canadian Rockies). J Metamorph Geol 6:297–309
Iiyama JT (1964) Etude des réactions d'échange d'ions Na-K dans la série muscovite-paragonite. Bull Soc Fr Mineral Crust 87:532–541
Jiang WT, Essene EJ, Peacor DR (1990) Transmission electron microscopic study of coexisting pyrophyllite and muscovite: direct evidence for the metastability of illite. Clays Clay Miner 38(3):225–240
Jiang W, Peacor DR, Essene EJ (1992) Muscovite- and R1 illite-smectite-kaolinite intergrowth in the Eocene McAdams sandstone: Nonexistence of hydro-muscovite and implications for illite metastability. Geol Soc Am Abstr Progr 24(7):71
Jolivet L, Patriat M (1999) Ductile extension and the formation of the Aegean sea. In: Durand B, Jolivet L, Horvath F, Seranne M (eds) The Mediterranean basins; Tertiary extension within Alpine Orogen. Geol Soc Lond Spec Publ 156:427–456
Kohn MJ, Spear FS (1991a) Error propagation for barometers. 1. Accuracy and precision of experimentally located end-members reactions. Am Mineral 76:128–137
Kohn MJ, Spear FS (1991b) Error propagation for barometers. 2. Application to rocks. Am Mineral 76:138–147
Kretz R (1983) Symbols for rock-forming minerals. Am Mineral 68:277–279
Krogh EJ, Raheim A (1978) Temperature and pressure dependence of Fe-Mg partitioning between garnet and phengite, with particular reference to eclogites. Contrib Mineral Petrol 66:75–80
Lambert RSJ (1959) The mineralogy and metamorphism of the Moine schists of the Morar and Knoydart District of Inverness-shire. Trans R Soc Edinburgh 63:553–588
Leoni L, Marroni M, Sartori F, Tamponi M (1996) Metamorphic grade in the metapelites of the Internal Liguride Units (Northern Apennines, Italy). Eur J Mineral 8:35–50
Leoni L, Sartori F, Tamponi M (1998) Compositional variation in K-white micas and chlorites coexisting in Al-saturated metapelites under late diagenetic to low-grade metamorphic conditions (Internal Liguride Units, Northern Apennines, Italy). Eur J Mineral 10:1321–1339
Lieberman J, Petrakakis K (1991) TWEEQU thermobarometry: Analysis of uncertainties and application to granulites from the western Alaska and Austria. Can Mineral 29:857–887
Mäder UK, Percival JA, Berman RG (1994) Thermobarometry of garnet-clinopyroxene-hornblende granulites from the Kapuskasing structural zone. Can J Earth Sci 31:1134–1145
Massonne HJ (1995) Experimental and petrogenetic study of UHPM. In: Coleman RG, Wang X (eds) Ultrahigh pressure metamorphism. Cambridge University Press, pp 33–95
Massonne HJ, Schreyer W (1986) High-pressure syntheses and X-ray properties of white micas in the system K_2O-MgO-Al_2O_3-SiO_2-H_2O. Neues Jahrb Mineral Abh 153:177–215
Massonne HJ, Schreyer W (1987) Phengite geobarometry based on the limiting assemblage with K-feldspar, phlogopite and quartz. Contrib Mineral Petrol 96:212–224
Massonne HJ, Schreyer W (1989) Stability field of the high-pressure talc-phengite and two new phengite barometers. Eur J Mineral 1:391–410
Massonne HJ, Szpurka Z (1997) Thermodynamic properties of white micas on the basis of high-pressure experiments in the systems K_2O-MgO-Al_2O_3-SiO_2-H_2O. Lithos 41:229–250
McMullin DWA, Berman RG, Greenwood HJ (1991) Calibration of the SGAM thermobarometer for pelitic rocks using data from phase-equilibrium experiments and natural assemblages. Can Mineral 29:889–908
Nenggao H, Jiaxi Y, Sanyuan A, Jianmin H (1993) Metamorphism and tectonic evolution of the Shangdan fault zone, Shaanxi, China. J Metamorph Geol 11:537–548
Okay AI, Kelley SP (1994) Tectonic setting, petrology and geochronology of jadeite + glaucophane and chloritoid + glaucophane schists from north-west Turkey. J Metamorph Geol 12:455–466
Parra T, Vidal O, Jolivet L (2002) Relation between deformation and retrogression in blueschist metapelites of Tinos Island (Greece), evidenced by chlorite-phengite local equilibria. Lithos 63:41–66
Patriat M (1996) Etude de la transition fragile-ductile, application au transect Olympe-Naxos, Grèce. Thèse Géologie, Université de Paris VI Jussieu
Pigage LC (1976) Metamporphism of the Settler Schist, southwest of Yale, British Columbia. Can J Earth Sci 13:405–421
Pigage LC (1982) Linear regression analysis of sillimanite-forming reactions at Azure Lake, British Columbia. Can Mineral 20:349–378
Pigage LC, Greenwood HJ (1982) Consistent estimates of pressure and temperature; the staurolite problem. Am J Sci 282(7):943–969
Radvanec M, Banno S, Okamoto K (1994) Multiples stages of phengite formation in sanbagawa schists. Contrib Mineral Petrol 51:37–48
Rieder M, Cavazzini G, D'Yakonov YS, Franck-Kamenetskii VA, Gottardi G, Guggenheim S, Koval PV, Muller G, Neiva AMR, Radoslovich EW, Robert JL, Takeda H, Weiss Z, Jones DR (1998) Nomenclature of the micas. Can Mineral 36:905–912
Rothbauer R (1971) Untersuchung eines 2M1 Muskovits mit Neutronenstrahlen. Neues Jahrb Mineral Monatsh:143–154
Roux J, Hovis GL (1996) Thermodynamic mixing models for muscovite-paragonite solutions based on solution calorimetric and phase equilibrium data. J Petrol 37(5):1241–1254
Schmidt MW (1998) La déshydratation dans les zones de subduction et le recyclage des matériaux crustaux dans le manteau. Thèse Habilitation, Université Blaise-Pascal, Clermont-Ferrand

Theye T, Seidel E (1991) Petrology of low-grade high-pressure metapelites from the Extemal Hellenides (Crete, Peloponnese). A case study with attention to sodic minerals. Eur J Mineral 3:343–366

Tracy RJ (1978) High grade metamorphic reactions and partial melting in pelitic schists, west-central Massachusetts. Am J Sci 278:150–178

Trotet F, Vidal O, Jolivet L (2001a) Exhumation of Syros and Sifnos metamorphic rocks (Cyclades, Greece). New constraints on the P-T paths. Eur J Mineral 13(5):901–920

Trotet F, Jolivet L, Vidal O (2001b) Tectono-metamorphic evolution of Syros and Sifnos Islands (Cyclades, Greece). Tectonophysics 2(338):179–206

Velde B (1965) Phengite micas: synthesis, stability, and natural occurrence. Am J Sci 263:886–913

Vidal O, Parra T (2000) Exhumation paths of high pressure metapelites obtained from local equilibria for chlorite-phengite assemblages. Geol Mag 35:139–161

Vidal O, Goffé B, Theye T (1992) Experimental study of the stability of sudoite and magnesiocarpholite and calculation of a new petrogenetic grid for the system FeO-MgO-$A1_2O_3$-SiO_2-H_2O. J Metamorph Geol 10:603–614

Vidal O, Theye T, Chopin C (1994) Experimental study of chloritoid stability at high pressure and various fO_2 conditions. Contrib Mineral Petrol 118:256–270

Vidal O, Goffé B, Parra T, Bousquet R (1999) Calibration and testing of an empirical chloritoid-chlorite Mg-Fe thermometer and thermodynamic data for daphnite. J Metamorph Geol 17:25–39

Vidal O, Parra T, Trotet F (2001) A thermodynamic model for Fe-Mg aluminous chlorite using data from phase equilibrium experiments and natural pelitic assemblages in the 100–600 °C, 1–25 kbar range. Am J Sci 6(301):557–592

Wang GF, Banno S (1987) Non-stoichiometry of interlayer cations in micas from low- to middle grade metamorphic rocks in the Ryoke and the Sambagawa belts, Japan. Contrib Mineral Petrol 97:313–319

Worley B, Powell R (2000) High-precision relative thermobarometry: theory and example. J Metamorph Geol 18:91–101

Worley B, Powell R, Wilson C (1997) Crenulation cleavage formation: Evolving diffusion, deformation and equilibration mechanisms with increasing metamorphic grade. J Struct Geol 19:1121–1135

Yates DM, Rosenberg PE (1993) Hydrothermal transformation of muscovite to end member illite at 250 °C. Geol Soc Am Abstr Progr A437

Yates DM, Rosenberg PE (1996) Formation and stability of end-member illite. I. Solution equilibration experiments at 100 to 150 °C and Pv, H_2O. Geochim Cosmochim Acta 60:1873–1883

Zen EA, Ross M, Bearth P (1964) Paragonite from Tasch Valley near Zermatt, Switzerland. Am Mineral 49:183–190

Zhang RY, Liou JG (1994) Coesite-bearing eclogite in Henan Province, central China: detailed petrography, glaucophane stability and P-T path. Eur J Mineral 6:217–233